iScience

CellPress
OPEN ACCESS

Article

# Annexin A1 exerts analgesic effect in a mouse model of medication overuse headache

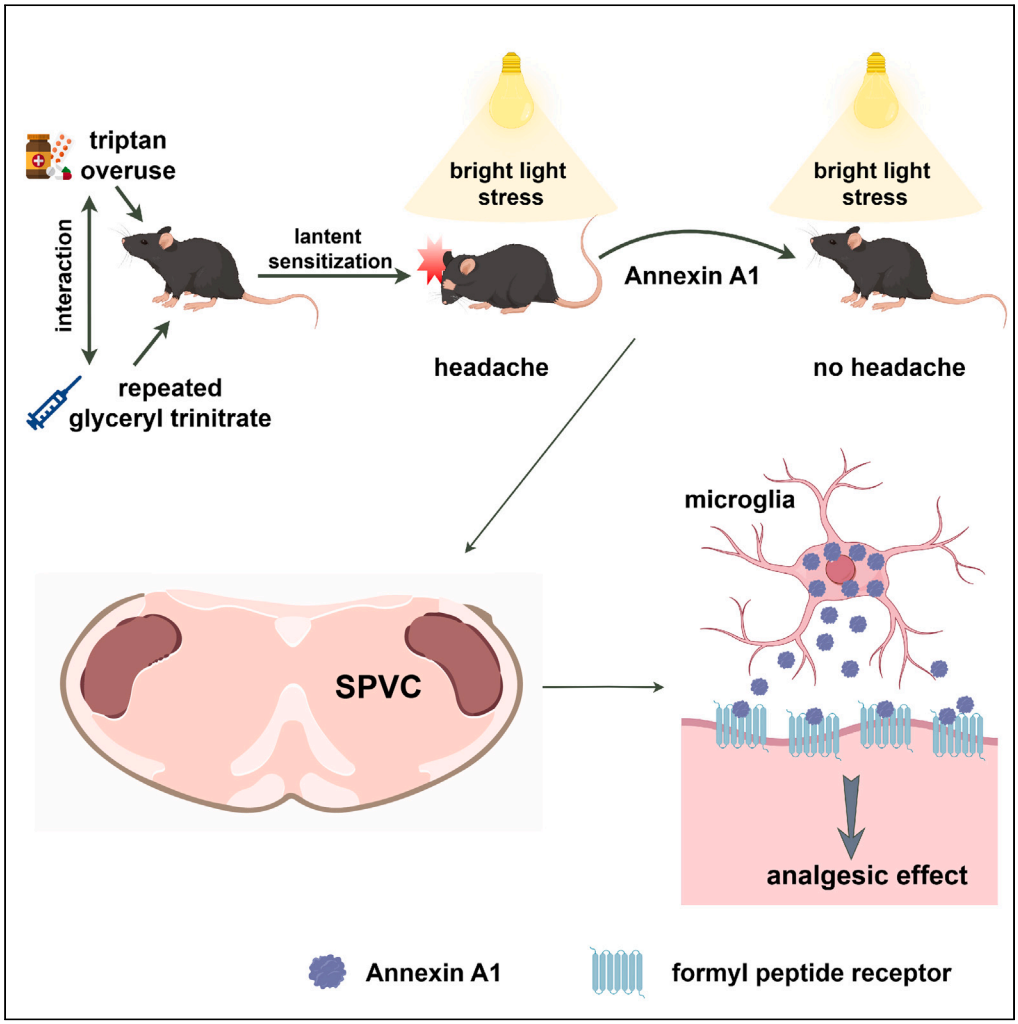


Zihua Gong, Chunxiao Yang, Wei Dai, ..., Xun Han, Shengyuan Yu, Zhao Dong

yusy1963@126.com (S.Y.)
dong_zhaozhao@126.com (Z.D.)

## Highlights

Triptan overuse aggravates allodynia and latent sensitization in migraine mice

Triptan overuse increases the expression of Annexin-A1 in the SPVC in migraine mice

Annexin-A1 exerts analgesic effect in migraine mice with triptan overuse

Annexin-A1 is a promising target for triptan associated medication overuse headache

Gong et al., iScience *26*, 108153
November 17, 2023 
https://doi.org/10.1016/j.isci.2023.108153

iScience

CellPress
OPEN ACCESS

Article

# Annexin A1 exerts analgesic effect in a mouse model of medication overuse headache

Zihua Gong,[1,2,3] Chunxiao Yang,[1,4] Wei Dai,[1] Shuai Miao,[1] Yingyuan Liu,[1,2] Zhiyang Jiao,[5] Bozhi Li,[1] Wei Xie,[1,2] Wei Zhao,[1,2] Xun Han,[1] Shengyuan Yu,[1,2,*] and Zhao Dong[1,2,6,*]

## SUMMARY

**Medication overuse headache (MOH) is a serious global condition. The interaction between headache attacks and medication overuse complicates the understanding of its pathophysiology. In this study, we developed a preclinical MOH model that incorporates these two key factors by overusing rizatriptan benzoate (RIZ, 4 mg/kg, i.g.) in a glyceryl trinitrate (GTN, 10 mg/kg, i.p.) induced chronic migraine mouse model. We observed that RIZ overuse aggravated GTN-induced cutaneous allodynia and caused a prolonged state of latent sensitization. We also detected a significant upregulation of Annexin-A1 (ANXA1), a protein mainly expressed in the microglia of the spinal trigeminal nucleus caudalis (SPVC), in GTN+RIZ mice. Intracerebroventricular injection of ANXA1-derived peptide Ac2-26 trifluoroacetic acid (TFA) (5 μg/mouse) inhibited bright light stress (BLS) induced acute allodynia via the formyl peptide receptor (FPR) in GTN+RIZ mice. These results suggest that ANXA1 may have an analgesic effect in triptan-associated MOH and could potentially serve as a therapeutic target.**

## INTRODUCTION

Migraine is a severe disabling neurological disorder affecting hundreds of millions of individuals worldwide. The treatment of acute headache attacks is an important part of the clinical management of migraine. However, frequent and excessive intake of acute anti-migraine drugs or analgesics can cause a new type of headache or significant worsening of pre-existing headache, known as medication overuse headache (MOH).[1] MOH is also a worldwide condition affecting about 100 million people[2] with a prevalence range of 1%–2%,[3] and is associated with substantial socioeconomic consequences.[4] Although MOH has been recognized for decades, the development of specific treatments has been slow, in part as a result of an incomplete understanding of its pathophysiology.

Existing clinical data suggest multiple factors may be involved in MOH pathophysiology, including central sensitization of the trigeminal and somatic nociceptive systems, abnormal spinal cord pain processing and cortical responses to somatosensory stimulation, and genetic predisposition.[5–9] Meanwhile, several preclinical MOH models have been developed by overusing analgesics alone, such as triptans, nonsteroidal anti-inflammatory drugs, opioids, and paracetamol, in normal animals. Studies using these models have explored the pathophysiology of MOH and found that prolonged analgesic administration can induce sensitization of pain pathways.[10–12] For instance, chronic exposure to opioids and triptans in rats has been shown to generalize cutaneous allodynia and create a state of latent sensitization to migraine triggers, such as environmental stress stimulus and nitric oxide (NO). These changes coexisted with an enhancement of the calcitonin gene-related peptide (CGRP) and neuronal NO synthase in trigeminal ganglion (TG) dural afferents.[11,12] Recent studies have shown that sustained sumatriptan exposure results in anomalous activation of the Nav1.9 channels in the TG by NO, thereby promoting MOH.[10] Other animal studies found that repeated exposure to acute migraine medication affected cortical excitability, including increased frequency of cortical spreading depression (CSD)[13,14] and decreased electrical stimulation threshold of CSD.[15] These preclinical studies provided important insights into the pathogenesis of MOH. However, the overuse of analgesics in normal animals, neglecting the role of pre-existing headache in MOH patients, may prevent more comprehensive investigation of the underlying pathophysiology of MOH.

The spinal trigeminal nucleus caudalis (SPVC), which contains second-order trigeminovascular neurons, plays a key role in the transmission of nociceptive signals and central sensitization in chronic headache.[16] However, the mechanism by which it contributes to the development of MOH remains unclear. Thus, the present study aimed to explore whether and how SPVC mediates the underlying molecular mechanism of MOH. To better mimic the clinical characteristics of MOH patients, we developed an MOH mouse model by overusing rizatriptan benzoate (RIZ) in a glyceryl trinitrate (GTN)-induced chronic migraine (CM) mouse model. RIZ is a 5-HT receptor agonist selective for 5-HT1D and

[1]Department of Neurology, The First Medical Center, Chinese PLA General Hospital, Beijing 100853, China
[2]Medical School of Chinese PLA, Beijing 100853, China
[3]Department of Medical Oncology, Bethune International peace Hospital, Shijiazhuang, Hebei 050082, China
[4]School of Medicine, Nankai University, Tianjin 300071, China
[5]Department of Outpatient, Shijiazhuang Fourth Retired Cadre Sanatorium of Hebei province Military Region, Shijiazhuang, Hebei 050082, China
[6]Lead contact
*Correspondence: yusy1963@126.com (S.Y.), dong_zhaozhao@126.com (Z.D.)
https://doi.org/10.1016/j.isci.2023.108153

5-HT1B subtypes and used for aborting migraine attack. The GTN-induced CM model is developed by repeated intraperitoneal injection of GTN in rodents and has been widely used for the investigation of migraine mechanisms and therapies because it can induce acute and chronic basal hyperalgesia and allodynia in rodents.[17–19] We validated this model with behavioral and histopathological experiments. We showed that chronic treatment with RIZ aggravated GTN-induced cutaneous allodynia and induced a prolonged state of latent sensitization accompanied by increased expression of c-Fos in the SPVC response to environmental stress stimulus. The RNA-seq results of SPVC revealed that RIZ alters the gene expression profiles in GTN mice. Further analysis and experiments showed that Annexin-A1 (ANXA1, formerly known as lipocortin-1) in the SPVC was upregulated by the overuse of RIZ in GTN mice.

ANXA1 is a member of the annexin superfamily of calcium-dependent phospholipid-binding proteins[20] that have multiple pathophysiological roles in inflammation, neurodegeneration, cancer, and endocrine control.[21] These biological effects of ANXA1 are mainly mediated through three G-protein coupled formyl peptide receptors (FPR1, FPR2, and FPR3).[21–23] Moreover, several studies have demonstrated the analgesic role of ANXA1 in inflammation-associated pain.[24–28] This analgesic effect is primarily achieved through an autocrine/paracrine mechanism involving FPR1 or FPR2. However, no studies have evaluated the potential role of ANXA1 and FPR in MOH or other headache types. In our present study, exogenous administration of ANXA1 can decrease the sensitivity of GTN+RIZ mice to environmental stress stimulus during prolonged latent sensitization. Our data proves that ANXA1 plays a critical role in the triptan-associated MOH.

## RESULTS

### Repeated administration of RIZ aggravates GTN-induced cutaneous allodynia

To investigate the effects of RIZ overuse on cutaneous allodynia in a GTN-induced CM model, we established the model by repeatedly administering intraperitoneal injections of GTN (10 mg/kg)[17] and simulated medication overuse by repeatedly administering intragastric doses of RIZ (4 mg/kg). The drugs were administered once every two days for a total of six doses, with the first day of administration being designated as day 0. Intraperitoneal injections were performed 30 min after gavage. To evaluate cutaneous allodynia, we measured the periorbital mechanical threshold (PMT) and the hindpaw mechanical threshold (HMT) prior to each drug administration. We referred to these measurements as the basal mechanical threshold. The PMT and HMT were measured every 2 days from day 0 until recovery (Figure 1A). Six repeated administrations of GTN+RIZ, GTN, or RIZ resulted in significant and time-dependent reductions in the basal PMT and HMT relative to the VEH+SAL group (Figure 1B). In addition, the basal PMT of GTN+RIZ-treated mice decreased significantly compared with VEH+RIZ treated mice from day 8, and the basal HMT of GTN+RIZ-treated mice was significantly lower than both GTN+SAL and VEH+RIZ-treated mice from day 8 (Figure 1B). Following the last dose of drugs, the PMT and HMT were continuously tested at 2-day intervals until they recovered to baseline levels of day 0 (i.e., no statistical difference compared with their own baseline levels of day 0). For the GTN+SAL and VEH+RIZ groups, the recovery occurred on day 18 and day 22, respectively, whereas the PMT and HMT of the GTN+RIZ treated mice took longer (day 26) to return to baseline levels (Figure 1C). These results demonstrate that consecutive treatment with RIZ aggravated GTN-induced chronic mechanical allodynia.

### Repeated administration of RIZ in GTN mice induces a prolonged state of latent sensitization

Latent sensitization is a state in which there is increased sensitivity to migraine triggers after sustained exposure to acute migraine medication. It has been proposed as a basal mechanism for the transformation of migraine to MOH.[12] After the mechanical thresholds of all groups returned to day 0 levels, mice were challenged with bright light stimulation (BLS) at an intensity of 3000 lux for 1 h on days 30 and 40 to investigate the effect of RIZ overuse in GTN mice on the duration of latent sensitization (Figure 1A). BLS is a known migraine trigger that has been reported to induce headache pain and activate trigeminal nociceptive neurons via a reflex circuit in the brainstem in naive rats at a threshold of 5000 lux.[29] Therefore, we hypothesized that a subthreshold light intensity (3000 lux) can induces acute mechanical allodynia in mice which is in a state of latent sensitization. The BLS challenge on day 30 elicited significant acute mechanical allodynia in the GTN+RIZ, GTN+SAL, and VEH+RIZ groups compared with the VEH+SAL group, peaking at 0.5 h and persisting for more than 3 h after BLS (Figure 2A). However, on day 40, only the GTN+RIZ group showed significant acute responses to BLS (Figure 2B), indicative of a prolonged state of latent sensitization. These data suggest that RIZ overuse can further prolong and exacerbate the increased vulnerability to migraine triggers of GTN mice.

### The number of BLS-responsive neurons in the SPVC is increased in GTN+RIZ treated mice on day 40

The immediate-early gene (e.g., c-Fos) has been extensively used as a marker for neurons respond to specific stimulations. In the SPVC, it provides an established readout of increased trigeminal nociception after noxious stimulation.[30,31] The superficial layer of the SPVC, which mainly receives input from nociceptive Aδ- and C-fibers, is especially sensitive to this effect.[32,33] Our results showed that chronic treatment with RIZ in GTN mice significantly increased the expression of c-Fos in both of the superficial and deeper layers of the SPVC post BLS by more than 300% compared with the other groups on day 40 (Figure 3). The increased BLS-responsive neurons in the SPVC suggest the GTN+RIZ mice still suffer a state of latent sensitization on day 40, and validated the behaviors results shown in Figure 2B, where only GTN+RIZ mice showed acute mechanical allodynia after BLS on day 40.

### GTN+RIZ alters the gene expression profiles in the SPVC

To probe the possible molecular mechanisms underlying the prolonged latent sensitization in GTN+RIZ mice, we harvested the bilateral entire SPVC tissue of the four mice groups on day 40 without BLS and analyzed their gene expression profiles using RNA-seq. The sequencing

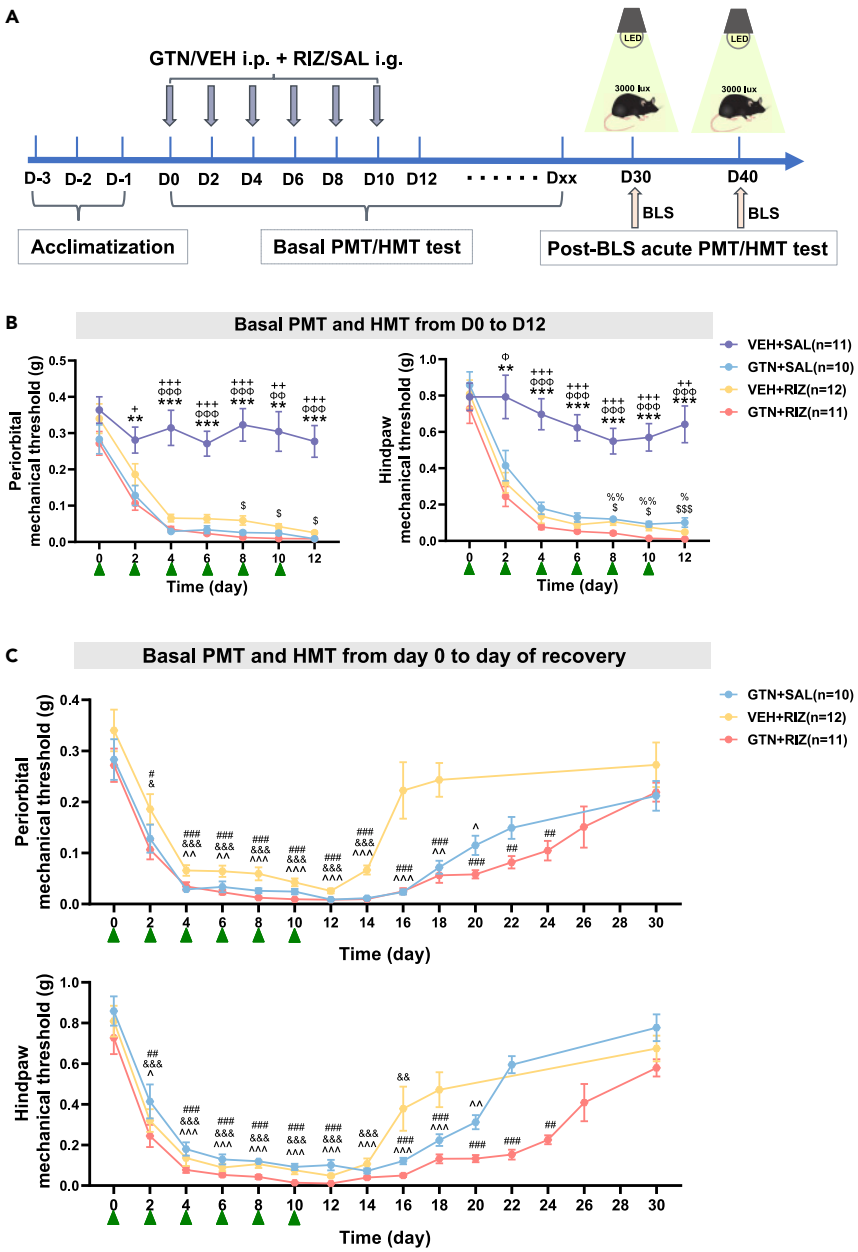


**Figure 1. Repeated administration of rizatriptan benzoate (RIZ) aggravates glyceryl trinitrate (GTN) induced cutaneous allodynia**

(A) Experimental flow chart for behavior test. PMT: periorbital mechanical threshold. HMT: hindpaw mechanical threshold. VEH: vehicle. SAL: saline. i.p.: intraperitoneally. i.g.: intragastrically. BLS: bright light stress. D: day. Dxx: day of recovery to D0 level.

(B) Characteristics of basal HMT and PMT changes over time among four groups from day 0-day 12. +p < 0.05, ++p < 0.01, +++p < 0.001 VEH+SAL group vs. GTN+SAL group. Φp < 0.05, ΦΦp <0.01, ΦΦΦp <0.001 VEH+SAL group vs. VEH+RIZ group. **p < 0.01, ***p < 0.001 VEH+SAL group vs. GTN+RIZ group. % p < 0.05, %% p < 0.01 GTN+RIZ group vs. GTN+SAL group. $p < 0.05, $$$p < 0.001 GTN+RIZ group vs. VEH+RIZ group. Two-way repeated-measures ANOVA with Tukey post hoc test: for PMT (left): main group effects: $F_{(3,40)} = 66.65$, $p < 0.0001$, main time effects: $F_{(3.578,\ 143.1)} = 43.67$, $p < 0.0001$. Interaction between group and time: $F_{(18,240)} = 3.061$, $p < 0.0001$; for HMT (right): main group effects: $F_{(3,40)} = 45.64$, $p < 0.0001$, main time effects: $F_{(3.25,130)} = 82.53$, $p < 0.0001$. Interaction between group and time: $F_{(18,240)} = 4.455$, $p < 0.0001$. Green triangles represent each administration of GTN/VEH+RIZ/SAL.

(C) Comparison of the time required for the recovery of HMT and PMT to baseline (day 0) among GTN+SAL, VEH+RIZ, and GTN+RIZ groups. &p < 0.05, &&p < 0.01, &&&p < 0.001 significantly reduced from the baseline within the VEH+RIZ group, One-way repeated-measures ANOVA with Dunnett post hoc test: for PMT: $F_{(3.038,\ 33.42)} = 19.70$, $p < 0.0001$, for HMT: $F_{(2.935,\ 32.29)} = 26.93$, $p < 0.0001$. ^p < 0.05, ^^p < 0.01, ^^^p < 0.001 significantly reduced from the baseline within the GTN+SAL group, One-way repeated-measures ANOVA with Dunnett post hoc test: for PMT: $F_{(3.406,\ 30.66)} = 23.12$, $p < 0.0001$, for HMT: $F_{(3.746,\ 33.71)} = 42.94$, $p < 0.0001$. #p < 0.05, ##p < 0.01, ###p < 0.001 significantly reduced from the baseline within the GTN+RIZ group, One-way repeated-measures ANOVA with Dunnett post hoc test: for PMT: $F_{(3.332,\ 33.32)} = 23.50$, $p < 0.0001$, for HMT: $F_{(2.867,\ 28.67)} = 34.07$, $p < 0.0001$. Data are represented as mean ± SEM.

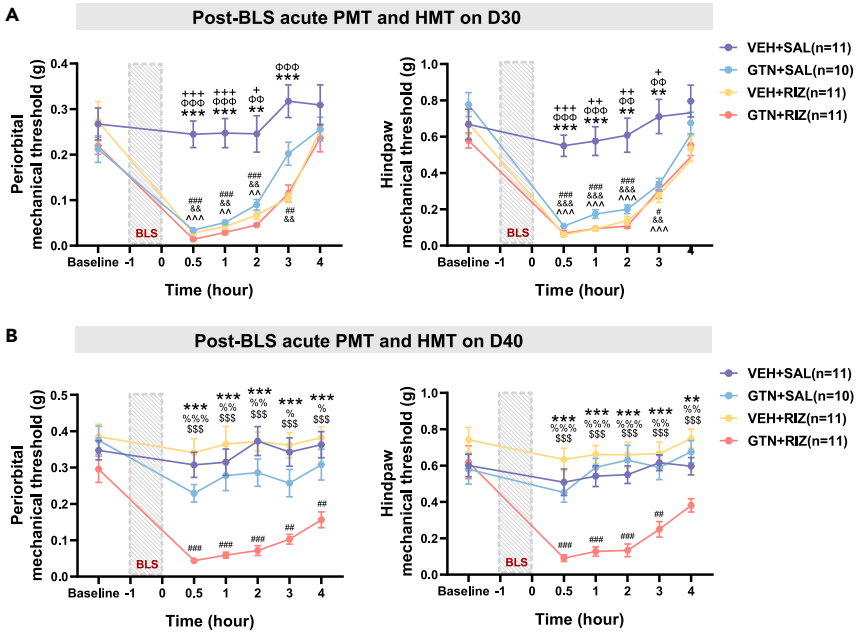


**Figure 2. Repeated administration of RIZ in GTN mice caused a prolonged state of latent sensitization**

(A) Comparisons of temporal characteristics of acute HMT and PMT responses to BLS among four groups on day 30. +p < 0.05, ++p < 0.01, +++p < 0.001 VEH+SAL group vs. GTN+SAL group. Φp < 0.05, ΦΦp <0.01, ΦΦΦp <0.001 VEH+SAL group vs. VEH+RIZ group. **p < 0.01, ***p < 0.001 VEH+SAL group vs. GTN+RIZ group. Two-way repeated-measures ANOVA with Tukey post hoc test: for PMT (left): main group effects: $F_{(3,39)} = 23.44$, p < 0.0001, main time effects: $F_{(3.553, 138.6)} = 57.87$, p < 0.0001. Interaction between group and time: $F_{(15, 195)} = 4.689$, p < 0.0001; for HMT (right): main group effects: $F_{(3,39)} = 20.7$, p < 0.0001, main time effects: $F_{(3.614, 141)} = 81.24$, p < 0.0001. Interaction between group and time: $F_{(15, 195)} = 5.370$, p < 0.0001. ^p < 0.05, ^^p < 0.01, ^^^p < 0.001 significantly reduced from the baseline within the GTN+SAL group. &p < 0.05, &&p < 0.01, &&&p < 0.001 significantly reduced from the baseline within the VEH+RIZ group, #p < 0.05, ##p < 0.01, ###p < 0.001 significantly reduced from the baseline within the GTN+RIZ group, One-way repeated-measures ANOVA with Dunnett post hoc test: for PMT (left): $F_{(1.228, 12.28)} = 34.53$ p < 0.0001, for HMT (right): $F_{(2.139, 21.39)} = 34.18$, p < 0.0001. #p < 0.05, ##p < 0.01, ###p < 0.001 significantly reduced from the baseline within the GTN+RIZ group, One-way repeated-measures ANOVA: for PMT (left): $F_{(2.075, 20.75)} = 41.96$, p < 0.0001, for HMT (right): $F_{(2.079, 20.79)} = 42.82$, p < 0.0001.

(B) Comparisons of temporal characteristics of acute HMT and PMT responses to BLS among four groups on day 40. *p < 0.05, **p < 0.01, ***p < 0.001 GTN+RIZ group vs. VEH+SAL group. %p < 0.05, %%p < 0.01, %%%p < 0.001 GTN+RIZ group vs. GTN+SAL group. $$p < 0.01, $$$p < 0.001 GTN+RIZ group vs. VEH+RIZ group. Two-way repeated-measures ANOVA with Tukey post hoc test: for PMT (left): main group effects: $F_{(3,39)} = 22.66$, p < 0.0001, main time effects: $F_{(3.559, 138.8)} = 11.26$, p < 0.0001. Interaction between group and time: $F_{(15, 195)} = 2.821$, p < 0.0001; for HMT (right): main group effects: $F_{(3, 39)} = 18.57$, p < 0.0001, main time effects: $F_{(3.811, 148.6)} = 13.38$, p < 0.0001. Interaction between group and time: $F_{(15, 195)} = 4.499$, p < 0.0001. #p < 0.05, ##p < 0.01, ###p < 0.001 significantly reduced from the baseline within the GTN+RIZ group, One-way repeated-measures ANOVA with Dunnett post hoc test: for PMT (left): $F_{(1.91, 19.1)} = 2.87$, p < 0.0001, for HMT (right): $F_{(1.597, 15.97)} = 26.09$, p < 0.0001. Data are represented as mean ± SEM.

produced approximately 40–60 million raw reads per sample. The clean reads Q20% and Q30% reached more than 97% and 92%, respectively (Table 1). In addition, over 91% of the clean reads were mapped to the mice genome (Table 1). Eventually, 56,270 transcripts were identified in the available expression genes from RNA-seq (Table S1). The previous results show that the library constructed in our study was of high enough quality and reliability to be used for subsequent bioinformatics analysis. We filtered out the differentially expressed genes (DEGs) between two groups with a criterion of adjusted p value < 0.05 and absolute fold change ≥ 2. The DEGs between two groups within four groups were then illustrated in six scatterplot graphs (Figure 4A). The total number of DEGs of the six comparable combinations is displayed in a histogram (Figure 4B). Most strikingly, repeated administration of RIZ to GTN mice led to the largest number of DEGs (including 234 up-regulated and 146 downregulated) in the SPVC compared with the VEH+SAL group (Figure 4B). To gain insights into the differences in gene expression patterns among the four groups, hierarchical clustering analysis was performed. Our results indicated that a clear segregation existed between the GTN+RIZ group and the other three groups (Figure 4C). These findings suggest that the differences in the SPVC gene transcription patterns may related to the prolonged latent sensitization in GTN+RIZ treated mice.

## Overuse of RIZ in GTN mice increases ANXA1 expression in the SPVC

To further probe the key DEGs involved in the molecular mechanisms underlying the prolonged latent sensitization in GTN+RIZ mice, we then performed Venn analysis on all six comparable combinations. We found a core set of 20 genes that were overlapped together among three comparable combinations (GTN+RIZ vs. VEH+SAL, GTN+RIZ vs. GTN+SAL, and GTN+RIZ vs. VEH+RIZ) (Figure 5A). Given that only GTN+RIZ mice showed acute allodynia to BLS on day 40, we assumed that the 20 overlapped DEGs in the GTN+RIZ group compared with the other

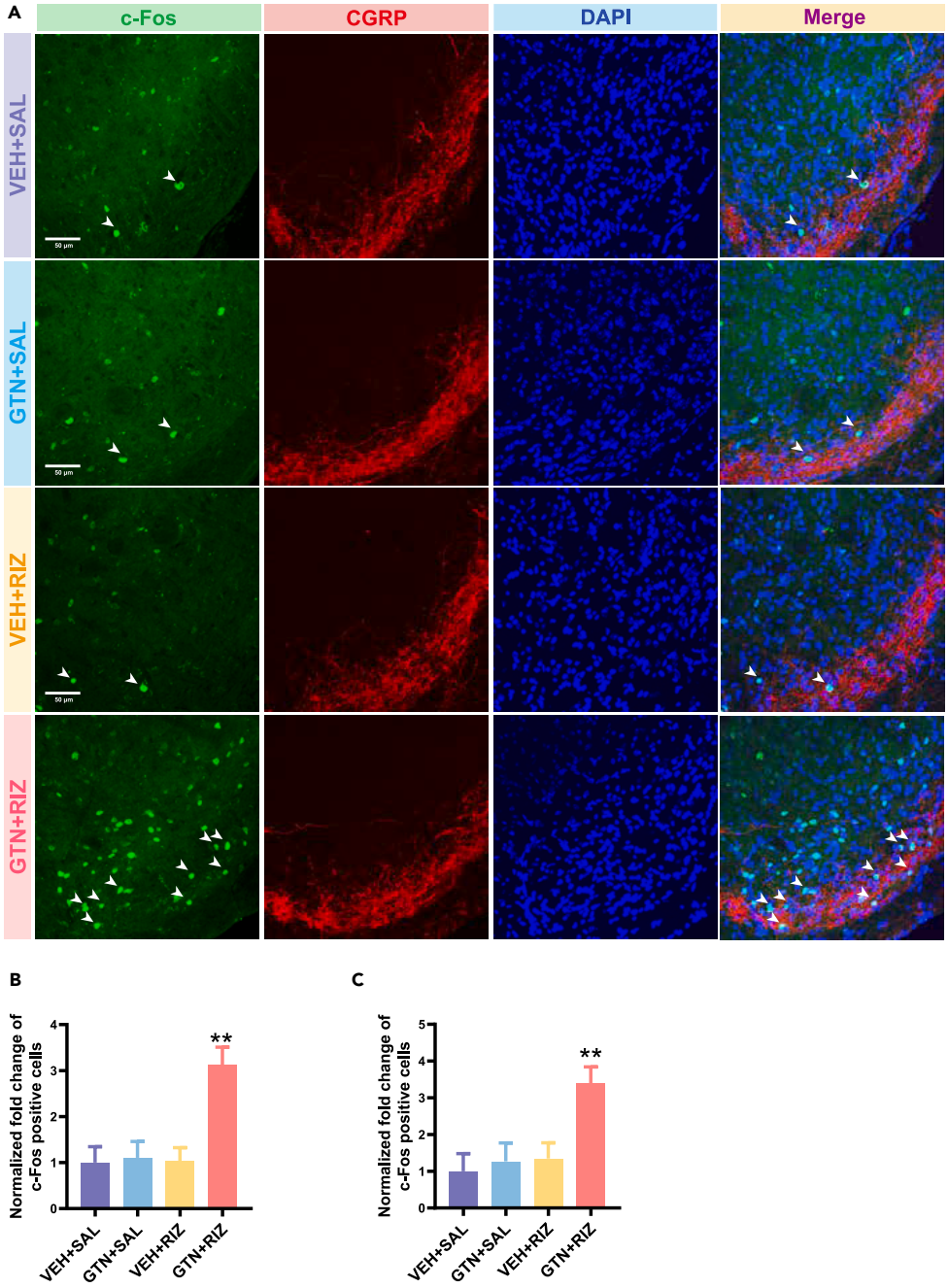


**Figure 3. Repeated administration of RIZ in GTN mice increases the expression of c-FOS in SPVC response to BLS on day 40**

(A) The representative images of c-FOS positive cells (green) and CGRP-immunoreactive staining (red) in SPVC from four groups. Scale bar, 50 μm.

(B) Fold changes in the number of c-FOS positive cells among four groups in superficial layers of the SPVC. **p < 0.01 GTN+RIZ group vs. other three groups. One-way ANOVA with Tukey post hoc test: $F_{(3, 8)} = 26.76$, p = 0.002. n = 4 mice per group.

(C) Fold changes in the number of c-FOS positive cells among four groups in deeper layers of the SPVC. **p < 0.01 GTN+RIZ group vs. other three groups, One-way ANOVA with Tukey post hoc test: $F_{(3, 8)} = 17.07$, p = 0.008. n = 4 mice per group. Data are represented as mean ± SEM.

three groups may contain the key DEGs which play a crucial role in the prolonged latent sensitization. We then conducted a hierarchical clustering analysis of these 20 genes and displayed the result in a heatmap. The results showed that there were 13 upregulated and 7 downregulated genes (Figure 5B). We then identified 3 of the 20 genes, namely, *Anxa1*, *Ctse*, and *Tnfsf9*, previously known to be involved in several pathophysiological processes, such as neuroinflammation, pain, and brain injury.[21,34,35] We further verified those three genes at the mRNA levels via quantitative real-time PCR (qRT-PCR), and the sequences of primer used in qRT-PCR test are listed in Table 2. We observed

**Table 1. The information of total reads for 20 samples in RNA-Seq**

| Sample | Raw reads | Clean reads | Q20 | Q30 | Total mapping ratio |
|---|---|---|---|---|---|
| VEH+SAL1 | 46364052 | 45526184 | 97.12% | 92.19% | 91.75% |
| VEH+SAL2 | 43347624 | 42723334 | 97.42% | 92.87% | 91.06% |
| VEH+SAL3 | 42544234 | 41677210 | 97.48% | 93.02% | 92.92% |
| VEH+SAL4 | 48219202 | 46873332 | 97.46% | 93.02% | 92.96% |
| VEH+SAL5 | 48252082 | 46871826 | 97.42% | 92.91% | 92.40% |
| GTN+SAL1 | 42592894 | 41924880 | 97.15% | 92.24% | 91.79% |
| GTN+SAL2 | 50024156 | 48176852 | 97.06% | 92.11% | 92.22% |
| GTN+SAL3 | 44432266 | 43482770 | 96.89% | 91.72% | 92.34% |
| GTN+SAL4 | 41833498 | 40794792 | 97.07% | 92.07% | 91.25% |
| GTN+SAL5 | 46251142 | 44950992 | 96.97% | 91.99% | 91.75% |
| GTN+RIZ1 | 42450534 | 40224730 | 97.30% | 92.71% | 92.92% |
| GTN+RIZ2 | 43457316 | 42602950 | 97.24% | 92.49% | 91.51% |
| GTN+RIZ3 | 40269634 | 38972230 | 97.42% | 92.94% | 92.14% |
| GTN+RIZ4 | 44683006 | 43979394 | 97.48% | 92.99% | 90.76% |
| GTN+RIZ5 | 45805608 | 45055872 | 97.13% | 92.26% | 95.05% |
| VEH+RIZ1 | 43726554 | 42866586 | 97.51% | 93.10% | 91.99% |
| VEH+RIZ2 | 45247948 | 44241210 | 97.18% | 92.32% | 92.32% |
| VEH+RIZ3 | 44792326 | 44111330 | 97.06% | 92.02% | 91.43% |
| VEH+RIZ4 | 55048904 | 53073048 | 97.12% | 92.23% | 92.52% |
| VEH+RIZ5 | 57465506 | 55257492 | 97.43% | 92.94% | 92.83% |

Q20 and Q30: the percentage of bases with a Phred value greater than 20 and 30, respectively in the total bases, where Phred = −10log10 (e). n = 5 mice per group.

a significant upregulation of only *Anxa1* in GTN+RIZ mice (Figures 5C–5E). The relative *Anxa1* mRNA level was 1.808 ± 0.571, 2.158 ± 0.741, 2.843 ± 0.799, and 16.77 ± 5.251 for VEH+SAL, GTN+SAL, VEH+RIZ, and GTN+RIZ group, respectively. Western blotting further confirmed that the protein expression of ANXA1 were significantly increased by more than two times in the SPVC of GTN+RIZ mice compared with the other three groups (Figure 5F). Given the important role of SPVC in the headache signal transmission and processing, our data suggest that ANXA1 may be involved in regulating headache signal during the prolonged latent sensitization in GTN+RIZ mice.

## ANXA1 is mainly expressed in microglia in the SPVC

We then characterized the expression profile of ANXA1 in the SPVC using dual-labeling immunofluorescence. The results revealed that ANXA1 immunoreactivity was highly co-expressed with ionized calcium-binding adapter molecule 1 (Iba1, 87.9%) and sparsely co-expressed with either neuronal nuclear antigen (NeuN, 4.7%) and glial fibrillary acidic protein (GFAP, 0.6%) (Figures 6A and 6B). In addition, we found ANXA1 was mainly expressed in the cytoplasm (78.5%) rather than nucleus (21.5%) within the microglia (Figure 6C).

## ANXA1 decreases the sensitivity to BLS in GTN+RIZ mice via FPR

We further explored the role of ANXA1 in prolonged latent sensitization in GTN+RIZ mice by intracerebroventricular injection of Ac2-26 TFA (an active N-terminal derived peptide of ANXA1, 5 μg/mouse)[24] and Boc-MLF TFA (a specific FPR antagonist, 1 μg/mouse) before BLS on day 40. The PMT and HMT were then tested 0.5 h after BLS. Saline was injected as control (Figure 7A). Consistent with our results in Figure 2B, saline-treated GTN+RIZ mice exhibited significant acute mechanical allodynia (Figures 7B and 7C), about three times lower than baseline in both PMT and HMT. Excitingly, pre-infusion of Ac2-26 TFA robustly reversed the decrease of PMT and prevented the decrease of HMT induced by BLS in GTN+RIZ mice. We then found that Boc-MLF TFA administered 15 min before Ac2-26 TFA injection, completely blocked the anti-nociceptive effectiveness of ANXA1-derived peptide, but with no effect on saline-treated GTN+RIZ mice (Figures 7B and 7C). Moreover, the data showed that pre-infusion of Ac2-26 TFA can significantly increase the PMT by about 1-folds in VEH+SAL mice. These results suggest a strong central anti-nociceptive effect of ANXA1 through modulation of the sensitivity of GTN+RIZ mice to BLS during the prolonged state of latent sensitization.

To further explore whether the analgesic effect of ANXA1 is related to c-Fos expression in SPVC, the c-Fos immunofluorescence experiment was conducted 2 h after the start of BLS. Our results showed that intracerebroventricular injection of Ac2-26 TFA significantly reduced the increased expression of c-Fos in the SPVC following BLS in GTN+RIZ mice on day 40 (Figure 8). Corresponding to the results shown in

**Table 2. Sequences of the primers used in qPCR**

| primers | Forward (5′–3′) | Reverse (5′–3′) |
|---|---|---|
| *Anxa1* | CACTCCAGCTTTCTTTGCCG | TAGTTTCCACCACACAGAGCC |
| *Ctse* | TGATGTTCTGCTCCGAAGGC | CCGGCAGGATGTAGTCAGTT |
| *Tnfsf9* | CGAGAGAATAATGCAGACCAGGT | TGTGCCAGTTCAGAGTTGTATTG |
| *Gapdh* | GAAGGTCGGTGTGAACGGAT | CCCATTTGATGTTAGCGGGAT |

*Anxa1*, Annexin A1; *Ctse*, cathepsin E; *Tnfsf9*, tumor necrosis factor superfamily 9; *Gapdh*, glyceraldehyde-3-phosphate dehydrogenase.

Figures 7B and 7C, Boc-MLF TFA blocked this effect of Ac2-26 TFA. These data suggest that ANXA1 may mediate its analgesic effect by regulating the response of neurons in the SPVC to nociceptive stimulation.

## DISCUSSION

It is unknown how chronic analgesic overuse causes worsening of a pre-existing headache. Moreover, the interaction between headache attacks and medication overuse complicates the pathophysiology behind MOH. Therefore, a reliable preclinical model is necessary for studying the mechanisms underlying MOH. Any preclinical model should reasonably mimic the human disorder, although it is very difficult to completely translate human disease to animal models. In MOH, pre-existing headache and excessive intake of analgesics are two key factors that need to be included as clinical data showed that only patients with a headache history who use analgesics regularly are prone to develop chronic headache, not the ones without headache.[36,37]

In the present study, we developed and validated a preclinical MOH model by overusing RIZ in GTN-induced CM mice, which could better mimic MOH patients. Researchers in the headache field were attracted by GTN because of the finding of its ability to induce a delayed headache attack in 50–80% of migraine patients and sometimes healthy subjects with a family history of migraine.[38] GTN-induced headache meets the IHS diagnostic criteria for migraine in most cases.[38,39] Furthermore, triptans can abort the spontaneous-like attacks induced by GTN.[40] These features suggest that GTN may be a useful translational model for many aspects of human migraine. Researchers then discovered that systemic GTN can induce trigeminal and spinal hyperalgesia in rodents by activating central structures involved in pain modulation. This phenomenon resembles the trigeminal or general pain hypersensitivity associated with migraine pain.[41,42] GTN-treated mice are now a well-established and widely used experimental model of migraine.[17,18] Cephalic and extracephalic cutaneous allodynia is the most important behavioral indicator to estimate this model.

Although Min Su et al. developed a rat MOH model using a combination of dural inflammation-induced headaches and RIZ overuse, which resulted in severe hyperalgesia, their primary focus was on the state during drug administration.[43] To comprehensively evaluate our MOH model, we conducted a follow-up assessment of mechanical thresholds in each group after drug administration was terminated, in addition to evaluating cutaneous allodynia during drug exposure. Consistent with other research findings,[10–12,17,18,43] repeated administration of GTN or RIZ alone induced significant cephalic and extracephalic allodynia, which suggests a state of central sensitization. Moreover, our data also showed that GTN+RIZ induced more severe cutaneous allodynia in mice during the drug administration than GTN or RIZ alone. We have noted that the basal PMT of GTN+RIZ group is not different from GTN+SAL group. Since 0.008g is the minimum value that the von Frey test can measure, GTN+RIZ may produce lower PMT values that the von Frey test cannot detect. Therefore, the lack of difference in basal PMT between GTN+RIZ group and GTN+SAL group may result from the lowest limitation of the von Frey test. However, we also observed that GTN+RIZ caused the most persistent cutaneous allodynia after the termination of drug administration. In summary, our data indicated that the interaction between GTN-induced chronic headache and triptan overuse led to a deeper and longer state of central sensitization. Our findings are consistent with those of the 2017 migraine in America symptoms and treatment study (MAST).[44] It showed that in addition to more monthly headache days, higher migraine symptom severity and pain intensity scores, migraine sufferers with acute medication overuse had higher rates of cutaneous allodynia. Moreover, patients with CM who used medication frequently showed greater disability and worse 24 h pain relief outcomes.[45,46] In this respect, our animal model demonstrates the effects of acute medication overuse in exacerbating central sensitization in chronic headaches, which may contribute to the development of MOH.

Furthermore, our MOH model showed a prolonged state of latent sensitization in the BLS test. This behavioral response was further verified by the increased expression of c-Fos induced by BLS in the SPVC on day 40. The increased expression of c-Fos in the SPVC suggests the hypersensitivity of the trigeminal pathway to nociceptive stimulations, which is thought to be necessary for the transformation of MOH.[47] It is possible that the overuse of triptans aggravates GTN-induced neural adaptations in trigeminal nociceptive pathways, which may increase vulnerability to migraine triggers and account for the exacerbation and prolonged state of latent sensitization, at least to some extent. It is important to note that increased expression of c-Fos only suggests and does not prove changes in neuronal activity in the SPVC. Further electrophysiological experiments are needed to confirm the changes in excitability of neurons in the SPVC.

Since the second-order trigeminovascular neurons are located in the SPVC and are closely associated with headache transmission and processing, the changed gene expression pattern of the SPVC induced by RIZ overuse in GTN mice indicated molecular mechanisms underlying prolonged latent sensitization. Among the DEGs, we identified a crucial gene named ANXA1.

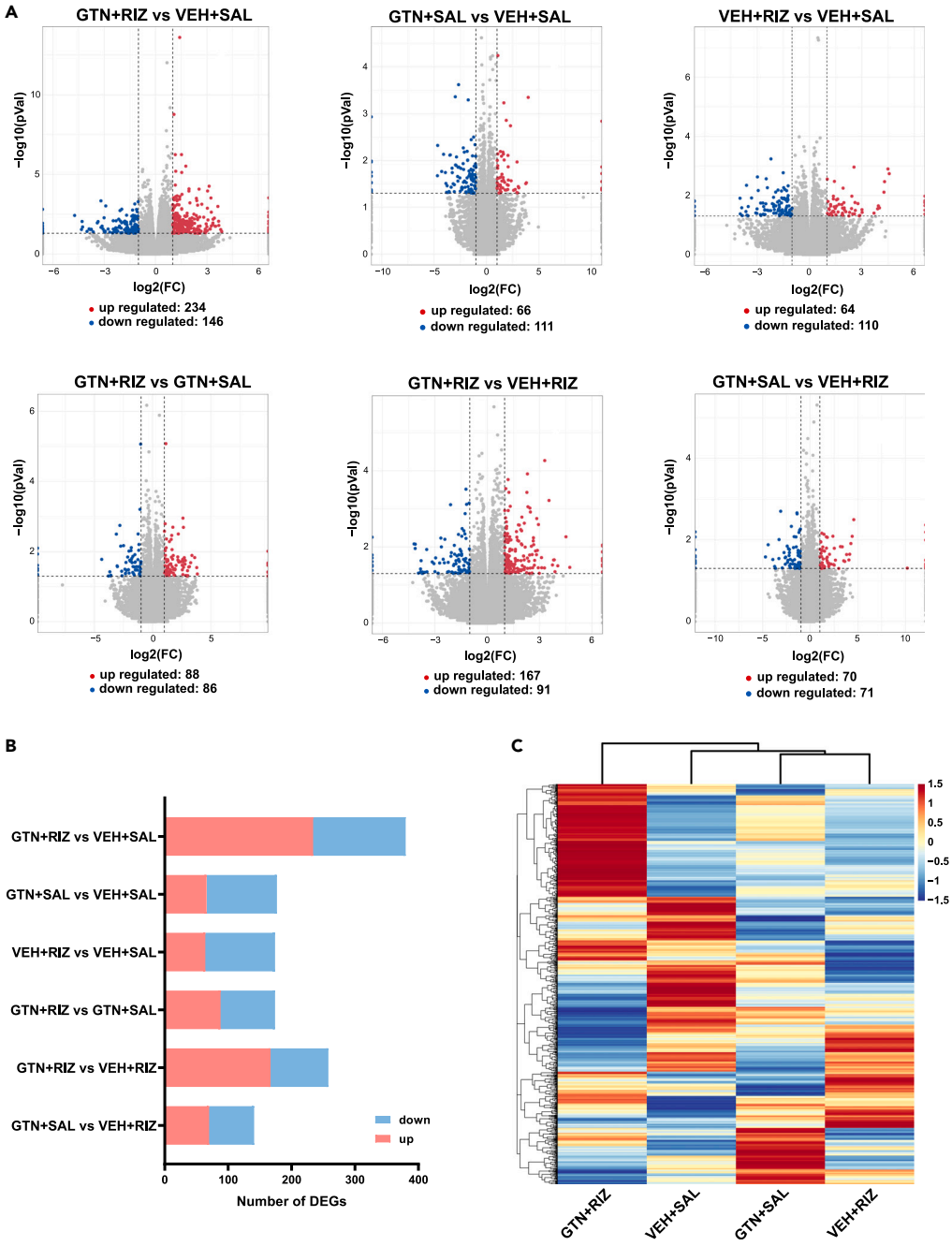


**Figure 4. RNA-seq of SPVC reveals the effect of RIZ on the gene expression profiles in GTN mice on day 40**

(A) Scatterplots showing gene expression profiles in SPVC of six comparable combinations. Red spots indicate upregulated DEGs, blue spots indicate downregulated DEGs, gray spots indicate non-DEGs.

(B) Summary of the number of DEGs of six comparable combinations.

(C) Heatmap displaying the hierarchical clustering of DEGs from four groups. n = 5 mice per group.

ANXA1 has been reported to exert its biological effects through translocating to nucleus to regulate DNA replication[48] and neuronal apoptosis,[49] or by binding to receptors on cell membranes to affect intracellular signal pathway.[21–23] In the central nervous system (CNS), ANXA1 has been reported to be expressed mainly in microglial cells.[49,50] In research related to pain or other CNS diseases, ANXA1 mainly mediates its pharmacological effects through an autocrine/paracrine mechanism involving FPR1 or FPR2.[24,25,51,52] It is upregulated and exerts anti-inflammatory effects in several neuroinflammation-associated diseases.[49,51–55] Meanwhile, neuroinflammation is thought to play an

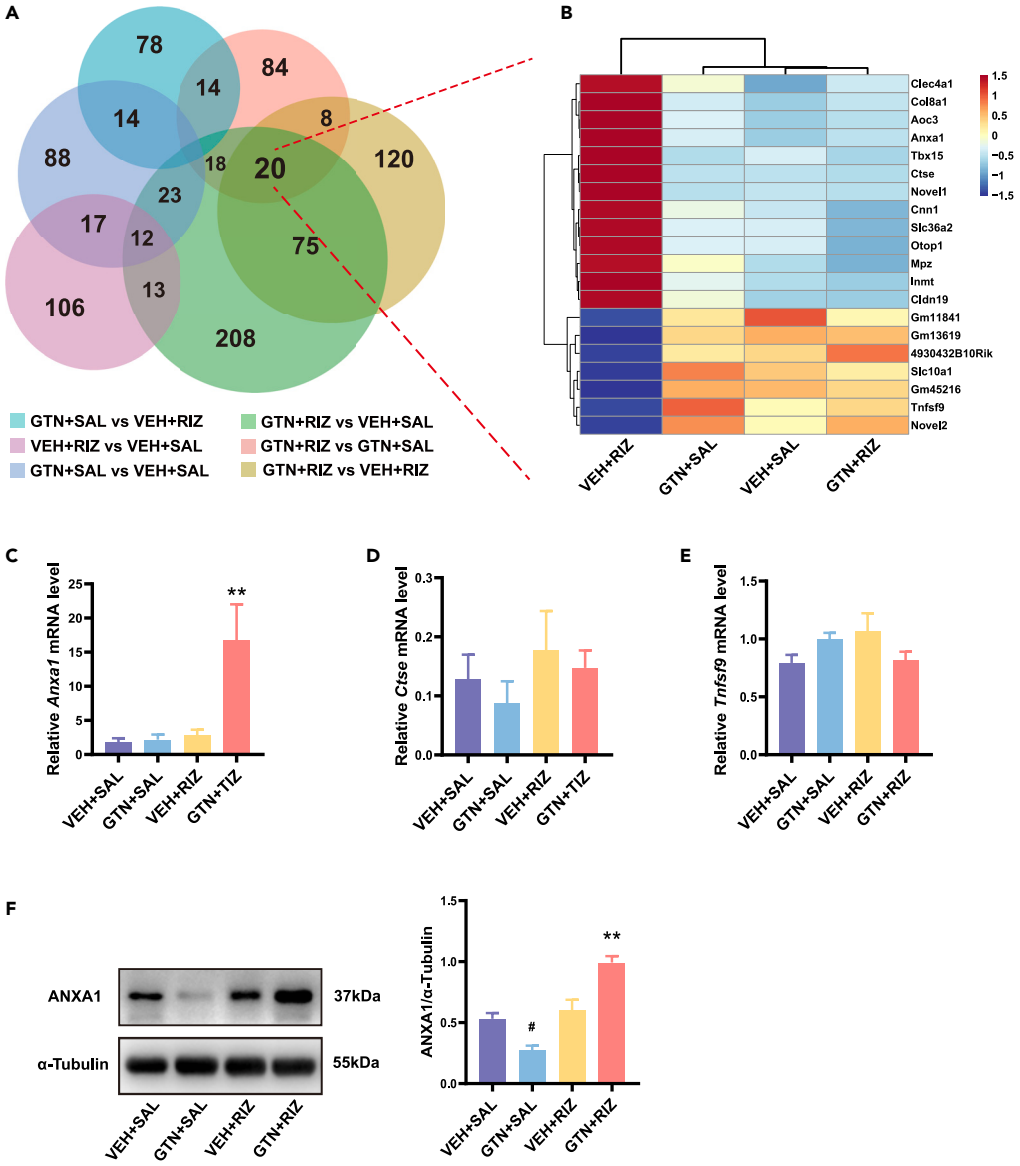


**Figure 5. ANXA1 significantly increased in SPVC in GTN+RIZ mice compared with the other three groups**

(A) Venn diagram showing the overlapping of DEGs in SPVC from six comparable combinations.

(B) Heatmap displaying the hierarchical clustering of 20 overlapping DEGs from four groups.

(C–E) Comparisons of relative *Anxa1*, *Ctse*, and *Tnfsf9* mRNA levels among four groups, respectively. **p < 0.01 GTN+RIZ group vs. other three groups, One-way ANOVA with Tukey post hoc test: C: $F_{(3,\ 12)} = 7.242$, p = 0.005; D: $F_{(3,\ 12)} = 0.6766$, p = 0.582; E: $F_{(3,\ 12)} = 1.956$, p = 0.174. n = 4 mice per group.

(F) Representative images of western blot results for ANXAI in SPVC and comparisons of relative ANXA1 protein level among four groups. **p < 0.01 GTN+RIZ group vs. other three groups. #p < 0.05 GTN+SAL group vs. other three groups. One-way ANOVA with Tukey post hoc test: $F_{(3,\ 8)} = 25.67$, p = 0.0002. n = 3 mice per group. Data are represented as mean ± SEM.

important role in the chronicity and central sensitization of migraine[56] and is likely associated with MOH transformation. The cellular localization of ANXA1 in our study confirmed that it was abundant in microglial cells in the SPVC and mainly expressed in the cytoplasm. Therefore, we supposed that the increased ANXA1 expression in GTN mice induced by triptan overuse might be due to an enhancing cytoplasmic synthesis and secretion of microglia in response to neuroinflammation. Similar to the findings of our study, pei Lei et al. found that ANXA1 was upregulated in L4/5 dorsal root ganglions in a rat model of inflammatory pain induced by complete Freund's adjuvant,[26] and ANXA1 mimic peptide Ac2-26 could inhibit nociception by desensitizing TRPV1 via the FPR2.[28] Here, we reported for the first time that ANXA1-derived peptide Ac2-26 TFA strongly decreased sensitivity to BLS in GTN+RIZ mice via the FPR during the state of latent sensitization. Moreover, Ac2-26 TFA can prevent the increased expression of c-Fos induced by BLS in the SPVC in GTN+RIZ mice. By inference, we propose that ANXA1 may

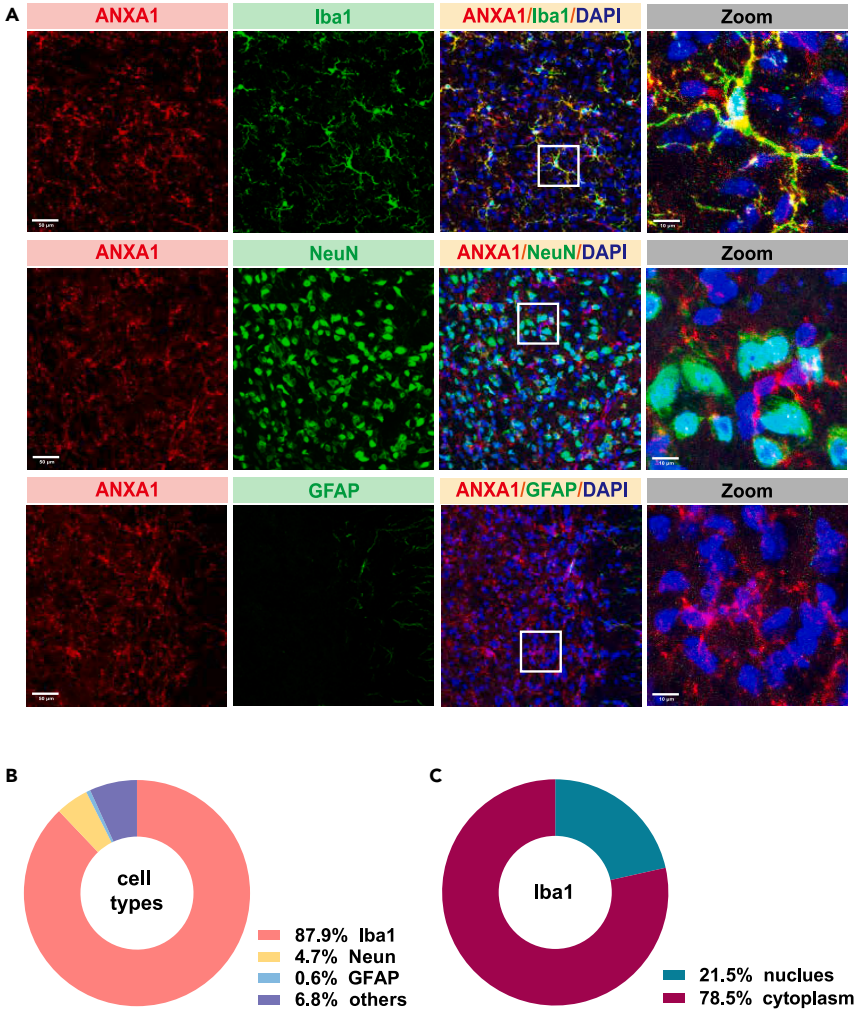


**Figure 6. ANXA1 is mainly expressed in microglial cells in SPVC**

(A) Representative co-labeling immunostaining images of ANXAI with Iba1, Neun, and GFAP in the SPVC (scale bar, 50 μm), white box, higher magnification close-ups (Right, scale bar, 10 μm).

(B) Quantitative analysis of overlapped immunoreactivity of ANXA1 with Iba1, Neun and GFAP.

(C) Quantitative analysis of nuclear and cytoplasmic ANXA1level within microglia. n = 3 mice per group.

exert a central anti-nociceptive effect by regulating headache signal transmission and processing pathway in some key nociceptive processing structures (e.g., the SPVC) via FPR during the development of MOH. However, additional experiments are needed in future to identify the exact brain region where ANXA1 produces its analgesic effect and which subtype of FPR involves in this anti-nociceptive effect.

In conclusion, we developed a preclinical model of MOH by repeated exposure of chronic migraine mice to medication, which could better mimic the clinical characteristics of patients with MOH. This is a promising mouse model for research of the transformation of MOH. More importantly, our findings indicate that ANXA1 in the CNS may contribute to modulating headache signal transmission and processing during prolonged latent sensitization in this MOH model. This may serve as a new target for exploring the pathophysiology and treatment of MOH.

## Limitations of the study

The limitation of our study is the absence of precise research methods, such as AAV-based RNA interference, to identify the specific brain region targeted by ANXA1. Additionally, due to the unavailability of suitable antibodies for FPR receptors in immunofluorescence staining, our study lacks data on the distribution of FPR in SPVC. Furthermore, we did not investigate the intracellular signal transduction process after ANXA1 binds to FPR. To reveal the specific mechanisms by which ANXA1 exerts central analgesia, further *in vitro* and *in vivo* studies are required.

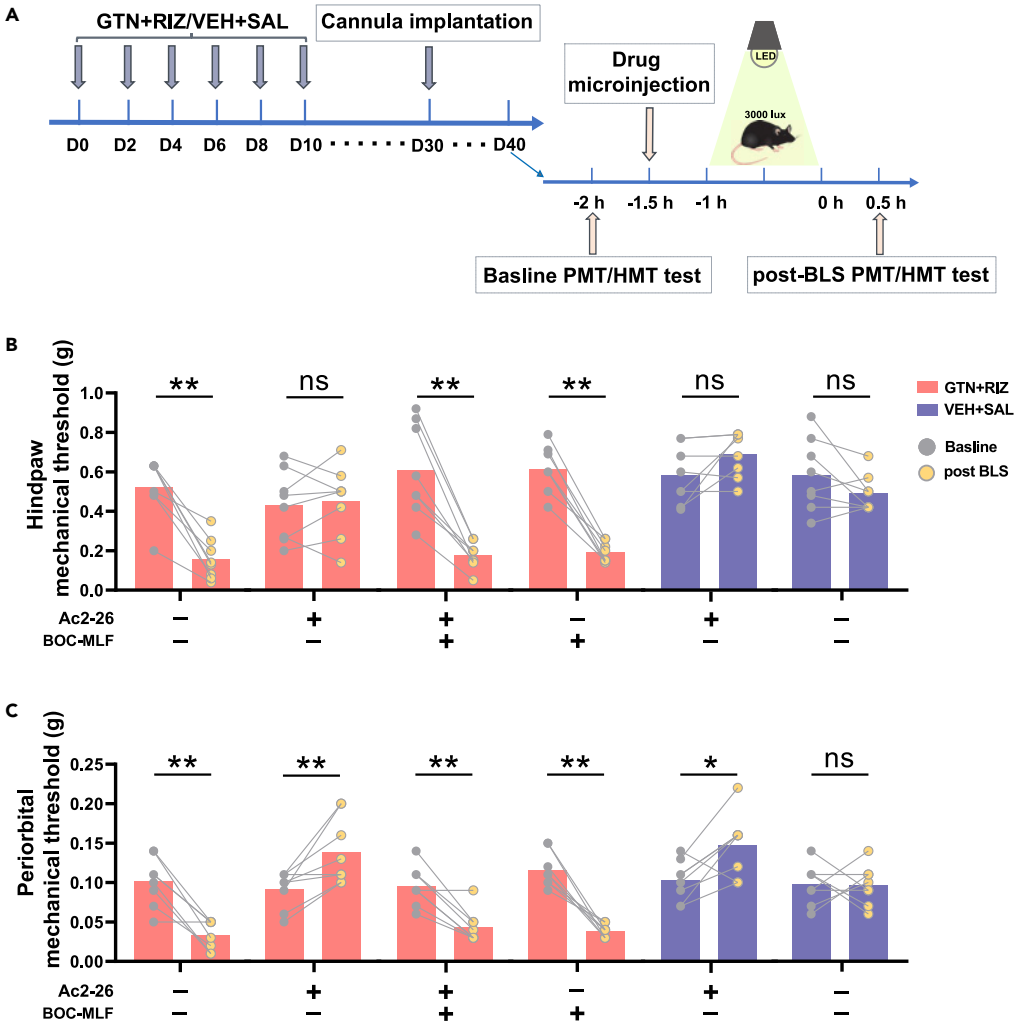


**Figure 7. Ac2-26 TFA exerts an analgesic effect in GTN+RIZ mice**

(A) Experimental flow chart for assessing the effect of ANXA1 on acute PMT and HMT response post BLS in GTN+RIZ mice on day 40.

(B and C) Effects of Ac2-26 TFA, saline and Boc-MLF TFA on acute HMT (B) and PMT (C) response post BLS in GTN+RIZ and VEH+SAL mice on day 40. *p < 0.05, **p < 0.01, paired *t* test: B: form left to right: $t_{(7)} = 6.593$, p = 0.003; $t_{(7)} = 0.4585$, p = 0.6605; $t_{(7)} = 6.316$, p = 0.004; $t_{(7)} = 10.43$, p < 0.0001; $t_{(7)} = 1.971$, p = 0.0893; $t_{(7)} = 1.647$, p = 0.1435. C: form left to right: $t_{(7)} = 5.665$, p = 0.008; $t_{(7)} = 3.60$, p = 0.0087; $t_{(7)} = 5.274$, p = 0.0012; $t_{(7)} = 7.785$, p = 0.0001; $t_{(7)} = 3.074$, p = 0.0180; $t_{(7)} = 0.08371$, p = 0.9356; n = 8 mice per group. Data are represented as mean ± SEM.

## STAR★METHODS

Detailed methods are provided in the online version of this paper and include the following:

- KEY RESOURCES TABLE
- RESOURCE AVAILABILITY
  - Lead contact
  - Materials availability
  - Data and code availability
- EXPERIMENTAL MODEL AND STUDY PARTICIPANT DETAILS
  - Animals
  - Institutional review board
  - Animal grouping and drug delivery
- METHOD DETAILS
  - Assessment of cutaneous allodynia

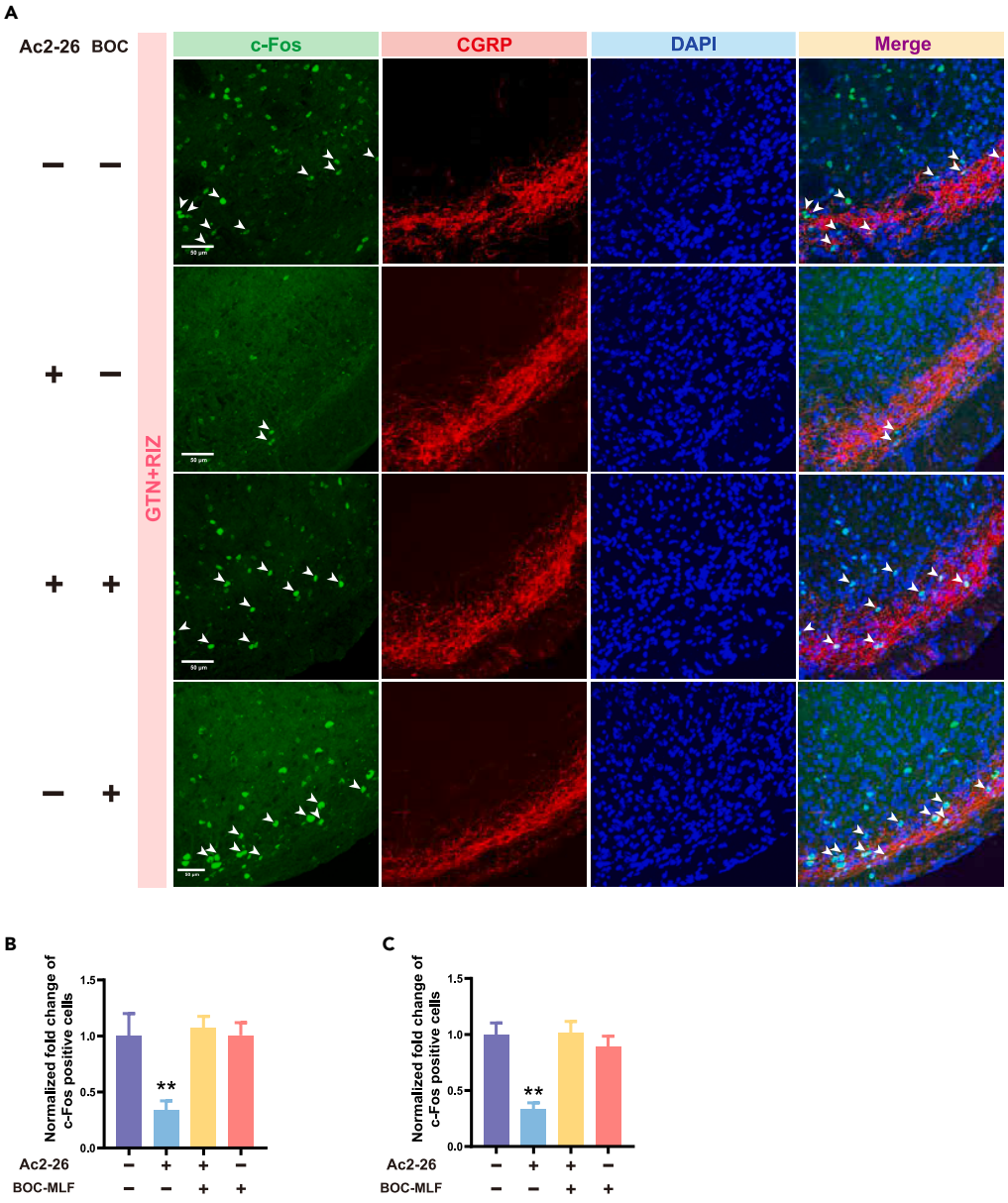


**Figure 8. Ac2-26 TFA decreases the expression of c-FOS in SPVC response to BLS on day 40**

(A) The representative images of c-FOS positive cells (green) and CGRP-immunoreactive staining (red) in SPVC from four groups. Scale bar, 50 μm.

(B) Fold changes in the number of c-FOS positive cells among four groups in superficial layers of the SPVC. **p < 0.01 Ac2-26 group vs. other three groups. One-way ANOVA with Tukey post hoc test: $F_{(3, 8)} = 20.37$, p = 0.0004. n = 3 mice per group.

(C) Fold changes in the number of c-FOS positive cells among four groups in deeper layers of the SPVC. **p < 0.01 Ac2-26 group vs. other three groups. One-way ANOVA with Tukey post hoc test: $F_{(3, 8)} = 38.38$, p < 0.0001. n = 3 mice per group. Data are represented as mean ± SEM.

- Latent sensitization test
- Immunofluorescence staining and imaging
- RNA-seq
- Differentially expressed gene analysis
- Quantitative RT-PCR
- Western blot
- Cannula implantation and drug intracerebroventricular microinjection

● QUANTIFICATION AND STATISTICAL ANALYSIS

## SUPPLEMENTAL INFORMATION

Supplemental information can be found online at https://doi.org/10.1016/j.isci.2023.108153.

## ACKNOWLEDGMENTS

Funding: This work is supported by the National Natural Science Foundation of China (grants 82171208 and 81771200 to Z.D. 82271242 to S.Y., 81901134 to X.H.), and the National Key Research and Development Program of China (grant 2022YFC2703600 to S.Y.).

## AUTHOR CONTRIBUTIONS

Z.G. responsible for performing the main experiments, drafting, and revising the manuscript. C.Y. and S.M. provided guidance for experimental design and revised the manuscript and figures. W.D. and Y.L. performed part of the behavioral tests. Z.J., B.L., and W.X. analyzed experimental data. W.Z. and X.H. provided technical and material support. Z.D. and S.Y. contributed equally as corresponding authors in providing overall direction of the project and funding support, editing the manuscript. All authors read and approved the final manuscript.

## DECLARATION OF INTERESTS

The authors declare no competing interests.

## INCLUSION AND DIVERSITY

We support inclusive, diverse, and equitable conduct of research.

Received: May 14, 2023
Revised: August 30, 2023
Accepted: October 3, 2023
Published: October 6, 2023

## REFERENCES

1. (2018). Headache Classification Committee of the International Headache Society (IHS) The International Classification of Headache Disorders, 3rd edition. Cephalalgia, 1–211. https://doi.org/10.1177/0333102417738202.
2. (2018). Global, regional, and national incidence, prevalence, and years lived with disability for 354 diseases and injuries for 195 countries and territories, 1990-2017: a systematic analysis for the Global Burden of Disease Study 2017. Lancet (London, England) *392*, 1789–1858. https://doi.org/10.1016/s0140-6736(18)32279-7.
3. Westergaard, M.L., Hansen, E.H., Glümer, C., Olesen, J., and Jensen, R.H. (2014). Definitions of medication-overuse headache in population-based studies and their implications on prevalence estimates: a systematic review. Cephalalgia *34*, 409–425. https://doi.org/10.1177/0333102413512033.
4. (2016). Global, regional, and national incidence, prevalence, and years lived with disability for 310 diseases and injuries, 1990-2015: a systematic analysis for the Global Burden of Disease Study 2015. Lancet (London, England) *388*, 1545–1602. https://doi.org/10.1016/s0140-6736(16)31678-6.
5. Ayzenberg, I., Obermann, M., Nyhuis, P., Gastpar, M., Limmroth, V., Diener, H.C., Kaube, H., and Katsarava, Z. (2006). Central sensitization of the trigeminal and somatic nociceptive systems in medication overuse headache mainly involves cerebral supraspinal structures. Cephalalgia *26*, 1106–1114. https://doi.org/10.1111/j.1468-2982.2006.01183.x.
6. Coppola, G., Currà, A., Di Lorenzo, C., Parisi, V., Gorini, M., Sava, S.L., Schoenen, J., and Pierelli, F. (2010). Abnormal cortical responses to somatosensory stimulation in medication-overuse headache. BMC Neurol. *10*, 126. https://doi.org/10.1186/1471-2377-10-126.
7. Perrotta, A., Serrao, M., Sandrini, G., Burstein, R., Sances, G., Rossi, P., Bartolo, M., Pierelli, F., and Nappi, G. (2010). Sensitisation of spinal cord pain processing in medication overuse headache involves supraspinal pain control. Cephalalgia *30*, 272–284. https://doi.org/10.1111/j.1468-2982.2009.01914.x.
8. Di Lorenzo, C., Coppola, G., Currà, A., Grieco, G., Santorelli, F.M., Lepre, C., Porretta, E., Pascale, E., and Pierelli, F. (2012). Cortical response to somatosensory stimulation in medication overuse headache patients is influenced by angiotensin converting enzyme (ACE) I/D genetic polymorphism. Cephalalgia *32*, 1189–1197. https://doi.org/10.1177/0333102412461890.
9. Di Lorenzo, C., Di Lorenzo, G., Sances, G., Ghiotto, N., Guaschino, E., Grieco, G.S., Santorelli, F.M., Casali, C., Troisi, A., Siracusano, A., and Pierelli, F. (2009). Drug consumption in medication overuse headache is influenced by brain-derived neurotrophic factor Val66Met polymorphism. J. Headache Pain *10*, 349–355. https://doi.org/10.1007/s10194-009-0136-0.
10. Bonnet, C., Hao, J., Osorio, N., Donnet, A., Penalba, V., Ruel, J., and Delmas, P. (2019). Maladaptive activation of Nav1.9 channels by nitric oxide causes triptan-induced medication overuse headache. Nat. Commun. *10*, 4253. https://doi.org/10.1038/s41467-019-12197-3.
11. De Felice, M., Ossipov, M.H., Wang, R., Dussor, G., Lai, J., Meng, I.D., Chichorro, J., Andrews, J.S., Rakhit, S., Maddaford, S., et al. (2010). Triptan-induced enhancement of neuronal nitric oxide synthase in trigeminal ganglion dural afferents underlies increased responsiveness to potential migraine triggers. Brain *133*, 2475–2488. https://doi.org/10.1093/brain/awq159.
12. De Felice, M., Ossipov, M.H., Wang, R., Lai, J., Chichorro, J., Meng, I., Dodick, D.W., Vanderah, T.W., Dussor, G., and Porreca, F. (2010). Triptan-induced latent sensitization: a possible basis for medication overuse headache. Ann. Neurol. *67*, 325–337. https://doi.org/10.1002/ana.21897.
13. Supornsilpchai, W., le Grand, S.M., and Srikiatkhachorn, A. (2010). Involvement of pro-nociceptive 5-HT2A receptor in the pathogenesis of medication-overuse headache. Headache *50*, 185–197. https://doi.org/10.1111/j.1526-4610.2009.01591.x.
14. Supornsilpchai, W., le Grand, S.M., and Srikiatkhachorn, A. (2010). Cortical hyperexcitability and mechanism of medication-overuse headache. Cephalalgia *30*, 1101–1109. https://doi.org/10.1177/0333102409355600.
15. Green, A.L., Gu, P., De Felice, M., Dodick, D., Ossipov, M.H., and Porreca, F. (2014). Increased susceptibility to cortical spreading depression in an animal model of medication-overuse headache. Cephalalgia *34*, 594–604. https://doi.org/10.1177/0333102413515344.
16. Ashina, M. (2020). Migraine. N. Engl. J. Med. *383*, 1866–1876. https://doi.org/10.1056/NEJMra1915327.
17. Pradhan, A.A., Smith, M.L., McGuire, B., Tarash, I., Evans, C.J., and Charles, A. (2014). Characterization of a novel model of chronic migraine. Pain *155*, 269–274. https://doi.org/10.1016/j.pain.2013.10.004.
18. Demartini, C., Greco, R., Zanaboni, A.M., Sances, G., De Icco, R., Borsook, D., and Tassorelli, C. (2019). Nitroglycerin as a comparative experimental model of migraine pain: From animal to human and back. Prog.

Neurobiol. *177*, 15–32. https://doi.org/10.1016/j.pneurobio.2019.02.002.
19. Akerman, S., Karsan, N., Bose, P., Hoffmann, J.R., Holland, P.R., Romero-Reyes, M., and Goadsby, P.J. (2019). Nitroglycerine triggers triptan-responsive cranial allodynia and trigeminal neuronal hypersensitivity. Brain *142*, 103–119. https://doi.org/10.1093/brain/awy313.
20. Crumpton, M.J., and Dedman, J.R. (1990). Protein terminology tangle. Nature *345*, 212. https://doi.org/10.1038/345212a0.
21. Sheikh, M.H., and Solito, E. (2018). Annexin A1: Uncovering the Many Talents of an Old Protein. Int. J. Mol. Sci. *19*, 1045. https://doi.org/10.3390/ijms19041045.
22. Serhan, C.N. (2007). Resolution phase of inflammation: novel endogenous anti-inflammatory and proresolving lipid mediators and pathways. Annu. Rev. Immunol. *25*, 101–137. https://doi.org/10.1146/annurev.immunol.25.022106.141647.
23. Ye, R.D., Boulay, F., Wang, J.M., Dahlgren, C., Gerard, C., Parmentier, M., Serhan, C.N., and Murphy, P.M. (2009). International Union of Basic and Clinical Pharmacology. LXXIII. Nomenclature for the formyl peptide receptor (FPR) family. Pharmacol. Rev. *61*, 119–161. https://doi.org/10.1124/pr.109.001578.
24. Pieretti, S., Di Giannuario, A., De Felice, M., Perretti, M., and Cirino, G. (2004). Stimulus-dependent specificity for annexin 1 inhibition of the inflammatory nociceptive response: the involvement of the receptor for formylated peptides. Pain *109*, 52–63. https://doi.org/10.1016/j.pain.2004.01.009.
25. Ayoub, S.S., Yazid, S., and Flower, R.J. (2008). Increased susceptibility of annexin-A1 null mice to nociceptive pain is indicative of a spinal antinociceptive action of annexin-A1. Br. J. Pharmacol. *154*, 1135–1142. https://doi.org/10.1038/bjp.2008.166.
26. Pei, L., Zhang, J., Zhao, F., Su, T., Wei, H., Tian, J., Li, M., and Shi, J. (2011). Annexin 1 exerts anti-nociceptive effects after peripheral inflammatory pain through formyl-peptide-receptor-like 1 in rat dorsal root ganglion. Br. J. Anaesth. *107*, 948–958. https://doi.org/10.1093/bja/aer299.
27. Luo, Z., Wang, H., Fang, S., Li, L., Li, X., Shi, J., Zhu, M., Tan, Z., and Lu, Z. (2020). Annexin-1 Mimetic Peptide Ac2-26 Suppresses Inflammatory Mediators in LPS-Induced Astrocytes and Ameliorates Pain Hypersensitivity in a Rat Model of Inflammatory Pain. Cell. Mol. Neurobiol. *40*, 569–585. https://doi.org/10.1007/s10571-019-00755-8.
28. Zhang, Y., Ma, S., Ke, X., Yi, Y., Yu, H., Yu, D., Li, Q., Shang, Y., Lu, Y., and Pei, L. (2021). The mechanism of Annexin A1 to modulate TRPV1 and nociception in dorsal root ganglion neurons. Cell Biosci. *11*, 167. https://doi.org/10.1186/s13578-021-00679-1.
29. Okamoto, K., Tashiro, A., Chang, Z., and Bereiter, D.A. (2010). Bright light activates a trigeminal nociceptive pathway. Pain *149*, 235–242. https://doi.org/10.1016/j.pain.2010.02.004.
30. Harriott, A.M., Strother, L.C., Vila-Pueyo, M., and Holland, P.R. (2019). Animal models of migraine and experimental techniques used to examine trigeminal sensory processing. J. Headache Pain *20*, 91. https://doi.org/10.1186/s10194-019-1043-7.
31. Bates, E.A., Nikai, T., Brennan, K.C., Fu, Y.H., Charles, A.C., Basbaum, A.I., Ptácek, L.J., and Ahn, A.H. (2010). Sumatriptan alleviates nitroglycerin-induced mechanical and thermal allodynia in mice. Cephalalgia *30*, 170–178. https://doi.org/10.1111/j.1468-2982.2009.01864.x.
32. Light, A.R., and Perl, E.R. (1979). Spinal termination of functionally identified primary afferent neurons with slowly conducting myelinated fibers. J. Comp. Neurol. *186*, 133–150. https://doi.org/10.1002/cne.901860203.
33. Kobayashi, M., and Nakaya, Y. (2020). Anatomical aspects of corticotrigeminal projections to the medullary dorsal horn. J. Oral Sci. *62*, 144–146. https://doi.org/10.2334/josnusd.19-0386.
34. Harada, Y., Zhang, J., Imari, K., Yamasaki, R., Ni, J., Wu, Z., Yamamoto, K., Kira, J.I., Nakanishi, H., and Hayashi, Y. (2019). Cathepsin E in neutrophils contributes to the generation of neuropathic pain in experimental autoimmune encephalomyelitis. Pain *160*, 2050–2062. https://doi.org/10.1097/j.pain.0000000000001596.
35. Yeo, Y.A., Martínez Gómez, J.M., Croxford, J.L., Gasser, S., Ling, E.A., and Schwarz, H. (2012). CD137 ligand activated microglia induces oligodendrocyte apoptosis via reactive oxygen species. J. Neuroinflammation *9*, 173. https://doi.org/10.1186/1742-2094-9-173.
36. Bahra, A., Walsh, M., Menon, S., and Goadsby, P.J. (2003). Does chronic daily headache arise de novo in association with regular use of analgesics? Headache *43*, 179–190. https://doi.org/10.1046/j.1526-4610.2003.03041.x.
37. Wilkinson, S.M., Becker, W.J., and Heine, J.A. (2001). Opiate use to control bowel motility may induce chronic daily headache in patients with migraine. Headache *41*, 303–309. https://doi.org/10.1046/j.1526-4610.2001.111006303.x.
38. Sances, G., Tassorelli, C., Pucci, E., Ghiotto, N., Sandrini, G., and Nappi, G. (2004). Reliability of the nitroglycerin provocative test in the diagnosis of neurovascular headaches. Cephalalgia *24*, 110–119. https://doi.org/10.1111/j.1468-2982.2004.00639.x.
39. Thomsen, L.L., Kruuse, C., Iversen, H.K., and Olesen, J. (1994). A nitric oxide donor (nitroglycerin) triggers genuine migraine attacks. Eur. J. Neurol. *1*, 73–80. https://doi.org/10.1111/j.1468-1331.1994.tb00053.x.
40. Vanmolkot, F., Van der Schueren, B., and de Hoon, J. (2006). Sumatriptan causes parallel decrease in plasma CGRP concentration and migraine headache during nitroglycerin-induced migraine attack. Cephalalgia *26*, 1037–1038. author reply 1038-1039. https://doi.org/10.1111/j.1468-2982.2006.01133_1.x.
41. Tassorelli, C., Joseph, S.A., Buzzi, M.G., and Nappi, G. (1999). The effects on the central nervous system of nitroglycerin–putative mechanisms and mediators. Prog. Neurobiol. *57*, 607–624. https://doi.org/10.1016/s0301-0082(98)00071-9.
42. Bernstein, C., and Burstein, R. (2012). Sensitization of the trigeminovascular pathway: perspective and implications to migraine pathophysiology. J. Clin. Neurol. *8*, 89–99. https://doi.org/10.3988/jcn.2012.8.2.89.
43. Su, M., Ran, Y., Han, X., Liu, Y., Zhang, X., Tan, Q., Li, R., and Yu, S. (2016). Rizatriptan overuse promotes hyperalgesia induced by dural inflammatory stimulation in rats by modulation of the serotonin system. Eur. J. Neurosci. *44*, 2129–2138. https://doi.org/10.1111/ejn.13296.
44. Schwedt, T.J., Alam, A., Reed, M.L., Fanning, K.M., Munjal, S., Buse, D.C., Dodick, D.W., and Lipton, R.B. (2018). Factors associated with acute medication overuse in people with migraine: results from the 2017 migraine in America symptoms and treatment (MAST) study. J. Headache Pain *19*, 38. https://doi.org/10.1186/s10194-018-0865-z.
45. Suh, G.I., Park, J.W., and Shin, H.E. (2012). Differences in Clinical Features and Disability according to the Frequency of Medication Use in Patients with Chronic Migraine. J. Clin. Neurol. *8*, 198–203. https://doi.org/10.3988/jcn.2012.8.3.198.
46. Lipton, R.B., Munjal, S., Buse, D.C., Fanning, K.M., Bennett, A., and Reed, M.L. (2016). Predicting Inadequate Response to Acute Migraine Medication: Results From the American Migraine Prevalence and Prevention (AMPP) Study. Headache *56*, 1635–1648. https://doi.org/10.1111/head.12941.
47. Sun-Edelstein, C., Rapoport, A.M., Rattanawong, W., and Srikiatkhachorn, A. (2021). The Evolution of Medication Overuse Headache: History, Pathophysiology and Clinical Update. CNS Drugs *35*, 545–565. https://doi.org/10.1007/s40263-021-00818-9.
48. Hirata, F., Thibodeau, L.M., and Hirata, A. (2010). Ubiquitination and SUMOylation of annexin A1 and helicase activity. Biochim. Biophys. Acta *1800*, 899–905. https://doi.org/10.1016/j.bbagen.2010.03.020.
49. Li, X., Xia, Q., Mao, M., Zhou, H., Zheng, L., Wang, Y., Zeng, Z., Yan, L., Zhao, Y., and Shi, J. (2021). Annexin-A1 SUMOylation regulates microglial polarization after cerebral ischemia by modulating IKKα stability via selective autophagy. Sci. Adv. *7*, eabc5539. https://doi.org/10.1126/sciadv.abc5539.
50. McKanna, J.A., and Zhang, M.Z. (1997). Immunohistochemical localization of lipocortin 1 in rat brain is sensitive to pH, freezing, and dehydration. J. Histochem. Cytochem. *45*, 527–538. https://doi.org/10.1177/002215549704500405.
51. Ding, Y., Flores, J., Klebe, D., Li, P., McBride, D.W., Tang, J., and Zhang, J.H. (2020). Annexin A1 attenuates neuroinflammation through FPR2/p38/COX-2 pathway after intracerebral hemorrhage in male mice. J. Neurosci. Res. *98*, 168–178. https://doi.org/10.1002/jnr.24478.
52. Schröder, N., Schaffrath, A., Welter, J.A., Putzka, T., Griep, A., Ziegler, P., Brandt, E., Samer, S., Heneka, M.T., Kaddatz, H., et al. (2020). Inhibition of formyl peptide receptors improves the outcome in a mouse model of Alzheimer disease. J. Neuroinflammation *17*, 131. https://doi.org/10.1186/s12974-020-01816-2.
53. Young, K.A., Hirst, W.D., Solito, E., and Wilkin, G.P. (1999). De novo expression of lipocortin-1 in reactive microglia and astrocytes in kainic acid lesioned rat cerebellum. Glia *26*, 333–343. https://doi.org/10.1002/(sici)1098-1136(199906)26:4<333::aid-glia7>3.0.co;2-s.
54. Ries, M., Loiola, R., Shah, U.N., Gentleman, S.M., Solito, E., and Sastre, M. (2016). The anti-inflammatory Annexin A1 induces the clearance and degradation of the amyloid-beta peptide. J. Neuroinflammation *13*, 234. https://doi.org/10.1186/s12974-016-0692-6.
55. Gimenes, A.D., Andrade, B.F.D., Pinotti, J.V.P., Oliani, S.M., Galvis-Alonso, O.Y., and Gil, C.D. (2019). Annexin A1-derived peptide

Ac(2-26) in a pilocarpine-induced status epilepticus model: anti-inflammatory and neuroprotective effects. J. Neuroinflammation *16*, 32. https://doi.org/10.1186/s12974-019-1414-7.

56. Edvinsson, L., Haanes, K.A., and Warfvinge, K. (2019). Does inflammation have a role in migraine? Nature reviews. Neurology *15*, 483–490. https://doi.org/10.1038/s41582-019-0216-y.

57. Christensen, S.L., Hansen, R.B., Storm, M.A., Olesen, J., Hansen, T.F., Ossipov, M., Izarzugaza, J.M.G., Porreca, F., and Kristensen, D.M. (2020). Von Frey testing revisited: Provision of an online algorithm for improved accuracy of 50% thresholds. Eur. J. Pain *24*, 783–790. https://doi.org/10.1002/ejp.1528.

58. Anders, S., Pyl, P.T., and Huber, W. (2015). HTSeq–a Python framework to work with high-throughput sequencing data. Bioinformatics *31*, 166–169. https://doi.org/10.1093/bioinformatics/btu638.

59. Anders, S., and Huber, W. (2010). Differential expression analysis for sequence count data. Genome Biol. *11*, R106. https://doi.org/10.1186/gb-2010-11-10-r106.

60. Chaplan, S.R., Bach, F.W., Pogrel, J.W., Chung, J.M., and Yaksh, T.L. (1994). Quantitative assessment of tactile allodynia in the rat paw. J. Neurosci. Methods *53*, 55–63. https://doi.org/10.1016/0165-0270(94)90144-9.

61. Navratilova, E., Behravesh, S., Oyarzo, J., Dodick, D.W., Banerjee, P., and Porreca, F. (2020). Ubrogepant does not induce latent sensitization in a preclinical model of medication overuse headache. Cephalalgia *40*, 892–902. https://doi.org/10.1177/0333102420938652.

62. Paxinos, G., and Franklin, K.B.J. (2001). The Mouse Brain in Stereotaxic Coordinates (Academic Press).

63. Saengjaroentham, C., Strother, L.C., Dripps, I., Sultan Jabir, M.R., Pradhan, A., Goadsby, P.J., and Holland, P.R. (2020). Differential medication overuse risk of novel anti-migraine therapeutics. Brain *143*, 2681–2688. https://doi.org/10.1093/brain/awaa211.

## STAR★METHODS

### KEY RESOURCES TABLE

| REAGENT or RESOURCE | SOURCE | IDENTIFIER |
|---|---|---|
| Antibodies | | |
| Rabbit monoclonal anti-c-Fos | Cell Signaling Technology | Cat#2250S; RRID: AB_2247211 |
| Goat polyclonal anti-CGRP | Abcam | Cat#ab36001; RRID: AB_725807 |
| Mouse monoclonal anti-Annexin-A1 | Santa Cruz Biotechnology | Cat#sc-12740; RRID: AB_2057007 |
| Rabbit monoclonal anti-Iba1 | Abcam | Cat#ab178846; RRID: AB_2636859 |
| Rabbit monoclonal anti-NeuN | Abcam | Cat#ab177487; RRID: AB_2532109 |
| Rabbit monoclonal anti-GFAP | Abcam | Cat#ab68428; RRID: AB_1209224 |
| Donkey anti-rabbit IgG H&L (Alexa Fluor® 488) preadsorbed | Abcam | Cat#ab150061; RRID: AB_2571722 |
| Goat anti-rabbit IgG H&L (Alexa Fluor® 488) preadsorbed | Abcam | Cat#ab150081; RRID: AB_2734747 |
| Donkey anti-goat IgG H&L (Alexa Fluor® 594) preadsorbed | Abcam | Cat#ab150136; RRID: AB_2782994 |
| Goat anti-mouse IgG H&L (Alexa Fluor® 594) preadsorbed | Abcam | Cat#ab150120; RRID: AB_2631447 |
| Rabbit monoclonal anti-Annexin-A1 | Abcam | Cat#ab214486; RRID: AB_2890907 |
| Mouse monoclonal anti-α-tubulin | Beyotime Biotechnology | Cat#AF2827 |
| HRP-labeled goat anti-mouse IgG (H + L) | Beyotime Biotechnology | Cat#A0216 |
| HRP-labeled goat anti-rabbit IgG (H + L) | Beyotime Biotechnology | Cat#A0208 |
| Chemicals, peptides, and recombinant proteins | | |
| Glyceryl trinitrate | Beijing Yimin Pharmaceutical Co., Ltd. | H11020289; CAS: 55-63-0 |
| Rizatriptan benzoate | Sichuan zitonggong pharmaceutical Co., Ltd. | H20060352; CAS: 145202-66-0 |
| 2,2,2-tribromoethanol | Sigma-Aldrich | Cat#T48402; CAS: 75-80-9 |
| 2-Methyl-2-butanol | Sigma-Aldrich | Cat#152463; CAS: 75-85-4 |
| TRIzol | Invitrogen | Cat#15596018; CAS: 9048-46-8 |
| Ac2-26 TFA | MedChemExpress | Cat#HY-P1098A |
| Boc-MLF TFA | MedChemExpress | Cat#HY-103473A |
| Evans Blue | Sigma-Aldrich | Cat#E2129; CAS: 314-13-6 |
| Critical commercial assays | | |
| O.C.T. TissueTek Compound | Sakura Finetek USA, Inc. | Cat#4583 |
| Mounting medium with DAPI | Abcam | Cat#ab104139 |
| NEBNext® Ultra™ RNA Library prep Kit for Illumina® | New England Biolabs | Cat#E7770 |
| USER Enzyme | New England Biolabs | Cat#M5505L |
| Phusion High-Fidelity DNA polymerase | New England Biolabs | Cat#M0530L |
| RNAprep FastPure Tissue &Cell Kit | TSINGKE | Cat#TSP413 |
| Goldenstar RT6 cDNA Synthesis Kit Ver.2 | TSINGKE | Cat#TSK302S |
| 2×T5 Fast qPCR Mix (SYBR Green I) | TSINGKE | Cat#TSE202 |
| RIPA lysis buffer | Beyotime Biotechnology | Cat# P0013B |
| Phenylmethylsulfonyl fluoride | Beyotime Biotechnology | Cat#ST506 |

(*Continued on next page*)

*Continued*

| REAGENT or RESOURCE | SOURCE | IDENTIFIER |
|---|---|---|
| Protease inhibitor | Roche | Cat#05892970001 |
| BCA protein Assay Kit | Beyotime Biotechnology | Cat#P0010S |
| 5× SDS-PAGE loading buffer | Beyotime Biotechnology | Cat#P0015L |
| Super ECL plus western blotting substrate | Wansheng Haotian Biotechnology Co., Ltd | Cat#EZWB01 |
| **Deposited data** | | |
| Raw RNA-seq data | This paper | SRA: PRJNA979279 |
| **Experimental models: Organisms/strains** | | |
| C57BL/6J mice | SPF (Beijing) Biotechnology Co., Ltd. | RRID: MGI: 2160531 |
| **Software and algorithms** | | |
| Algorithm for mechanical withdrawal thresholds | Christensen et al.[57] | https://bioapps.shinyapps.io/von_frey_app/ |
| ImageJ | NIH | https://imagej.net/software/fiji/ |
| HTSeq (v 0.13.5) | Anders et al.[58] | https://pypi.org/project/HTSeq/0.13.5/#files |
| DESeq R package (v 1.12.1) | Anders et al.[59] | https://www.bioconductor.org/packages//2.12/bioc/html/DESeq.html |
| OmicStudio tools | the Lianchuan Bioinformatics Cloud Platform | https://www.omicstudio.cn/tool |
| Graphpad prism 8 | Graphpad | https://www.graphpad.com/dL/1057948/D599DCF7/ |
| Adobe Illustrator 2022 | Adobe | https://www.adobe.com |
| **Other** | | |
| Calibrated von Frey monofilaments | Danmic Global | Cat#514000-20C |
| Freezing microtome | Leica Biosystems | Cat#CM1950 |
| Confocal microscope | Olympus | Cat#FV1000 |
| Illumina Novaseq 6000 platform | Illumina | N/A |
| Real-Time PCR System | Bioer Technology | Cat#FQD-96A |
| Homogenizer workcenter | IKA | Cat#0003737025 |
| Polyvinylidene difluoride membranes | Millipore | Cat# IPVH00010 |
| Tanon 5200 chemiluminescent imaging system | Tanon Science & Technology | N/A |
| Stereotaxic divice | RWD Life Science | Cat#69105 |
| Guide cannula | RWD Life Science | Cat#62003 |
| Injection cannula | RWD Life Science | Cat#62203 |
| Microliter syringe | Hamilton | Cat#1701 |
| Syringe pump | KD Scientific | Cat#788130 |

## RESOURCE AVAILABILITY

### Lead contact

- Further information and requests for resources and reagents should be directed to and will be fulfilled by the lead contact, Zhao Dong (dong_zhaozhao@126.com).

### Materials availability

- This study did not generate new unique reagents.

### Data and code availability

- Original RNA-seq data have been deposited at NCBI Sequence Read Archive and are publicly available as of the date of publication. Accession numbers are listed in the key resources table. Other data produced in this study are included in the published article and its supplemental information, or are available from the lead contact upon request.
- This paper does not report original code.
- Any additional information required to reanalyze the data reported in this paper is available from the lead contact upon request.

## EXPERIMENTAL MODEL AND STUDY PARTICIPANT DETAILS

### Animals

Only male mice were used in this study to minimize hormonal effects. Male C57BL/6J mice (8–10 weeks old, SPF (Beijing) Biotechnology Co., Ltd., Beijing, China) were group housed at room temperature of 23°C ± 2°C and humidity of 40%–60%. They were kept in a 12-h light-dark cycle with lights on at 08:00 p.m. and allowed access to food and water *ad libitum*.

### Institutional review board

The mice were used under protocols approved by the Institutional Animal Care and Use Committee of the Chinese people's Liberation Army General Hospital and according to Regulations for The Administration of Affairs Concerning Experimental Animals.

### Animal grouping and drug delivery

Glyceryl trinitrate (GTN, 5 mg/mL in absolute alcohol, Beijing Yimin pharmaceutical Co., Ltd., Beijing, China) was freshly diluted 15-fold with 0.9% saline for a dose of 10 mg/kg,[17] and an equal volume of 6.66% alcohol in saline was used as vehicle control. Rizatriptan benzoate (RIZ, Sichuan zitonggong pharmaceutical Co., Ltd., Sichuan, China) was diluted in 0.9% saline to a concentration of 2 mg/mL for a dose of 4 mg/kg, and an equal volume of 0.9% saline was used as control. The dose of RIZ was chosen based on our pilot study (Figure S1). Although 2 mg/kg, 4 mg/kg and 8 mg/kg RIZ can induce a significant decrease in basal HMT of mice from day 4 compared to saline, only the 4 mg/kg and 8 mg/kg groups show a significant acute decrease in HMT when mice were challenged with BLS on day 21 after the recovery of HMT. These data indicate that both 4 mg/kg and 8 mg/kg RIZ can induce both central sensitization and latent sensitization in mice. To avoid potential side effects caused by excessive drug dosage, we chose to use 4 mg/kg RIZ in our study. After 3 days of acclimatization to the von Frey test, 48 mice were randomly assigned to 4 groups: (1) GTN i.p.+RIZ i.g.; (2) GTN i.p.+SAL i.g.; (3) VEH i.p.+RIZ i.g.; (4) VEH i.p.+SAL i.g. The drugs were administered once every 2 days for a total of six doses. The day of first administration was taken as day 0 (Figure 1A). Intraperitoneal injections were performed 30 min after gavage. During the behavior experiment, four mice died from suffocation caused by wrong gavage and one mouse died from disease.

## METHOD DETAILS

### Assessment of cutaneous allodynia

Periorbital mechanical threshold (PMT) and hindpaw mechanical threshold (HMT) were measured using calibrated von Frey monofilaments (Aesthesio, 514000-20C, Danmic Global, San Jose, CA, USA; bending force ranging from 0.008 to 2 g) according to the up-and-down method[60] to evaluate cutaneous allodynia. In brief, the von Frey filaments were applied perpendicularly to the plantar surface of the hindpaw or the periorbital region until it buckled slightly to an "S" shape and held for 3–5 s or until a positive response occurred. If a negative response (O) was noted, the next greater force filament was applied, whereas if a positive response (X) was noted, a lighter filament was tested. Following the breaking point (XO/OX), four stimulations were applied to obtain the response pattern and final filament. Then, mechanical withdrawal thresholds were calculated using public domain algorithm (https://bioapps.shinyapps.io/von_frey_app/).[57] For the PMT test, the hair on the mouse's forehead (above and between the eyes) was shaved 7 days before testing. The mice were gently held in the palm of the experimenter with minimal restraint and the von Frey filaments were applied perpendicularly to the shaved skin. Swiping its face with the forepaw, shaking of the head and head withdrawal were registered as positives.[61] For the HMT test, mice were placed individually in a 10 cm × 7 cm × 16 cm (height) plexiglass chamber on a wire mesh floor and the plantar surface of the right hindpaw was chosen to stimulate with the von Frey filaments. The criteria for a positive response included swift withdrawal, shaking, or licking of the paw.[17] The mice were handled extensively or placed in plexiglass chambers to habituate to the von Frey test for 15–20 min daily on 3 consecutive days before the first testing day. The basal PMT and HMT were measured before the drug treatments every 2 days from day 0 to the day of recovery (Figure 1A).

### Latent sensitization test

After the recovery of basal PMT and HMT to day 0 levels, the mice were challenged with bright light stress (BLS) to evaluate latent sensitization. BLS was used to mimic a migraine trigger from environmental stressful stimulus.[11,61] In brief, the mice were placed individually in plexiglass cages and exposed to bright light (3000 lux) from a LED light placed on the top of the cage for 1 h. PMT and HMT were measured before BLS priming (baseline) and during a 4-h period after priming on day 30 and day 40 (Figure 1A).

### Immunofluorescence staining and imaging

On day 40, 2 h after the begining of BLS, the mice were anesthetized with 1.25% avertin (a mixture of 12.5 mg/mL of 2,2,2-tribromoethanol and 25 μL/mL 2-methyl-2-butanol, Sigma, T48402, 152463, St. Louis, MO, USA) at a dose of 0.2 mL/10g i.p. and transcardially perfused with 0.1M phosphate buffered saline (PBS) followed by 4% paraformaldehyde in PBS. Then the brains were removed, post-fixed in 4% paraformaldehyde, cryoprotected in 15% and 30% sucrose, embedded in O.C.T. TissueTekin Compound and sectioned coronally (30-μm slices) using a freezing microtome (Leica Biosystems, CM1950, Heidelberger, Germany). The free-floating sections were washed with PBS and then incubated with a blocking buffer (10% normal donkey serum and 0.25% Triton X-100 in PBS) for 2 h at room temperature. Sections were then incubated with primary antibody rabbit anti-c-Fos (1:1000, Cell Signaling Technology, 2250S, Danvers, MA, USA), goat anti-CGRP (1:500, Abcam, ab36001, Waltham, MA, USA), mouse anti-Annexin-A1 (1:500, Santa Cruz Biotechnology (Shanghai) Co., Ltd., sc-12740, Shanghai, China), and rabbit anti-Iba1(1:1000, Abcam, ab178846, Waltham, MA, USA), rabbit anti-NeuN (1:500, Abcam, ab177487, Waltham, MA, USA), rabbit anti-GFAP (1:500, Abcam, ab68428, Waltham, MA, USA) overnight at 4°C. On the next day, after washed thrice for 15 min each in PBS with 0.25% Triton X-100 (PBST), sections were incubated with donkey anti-rabbit or goat anti-rabbit IgG conjugated with Alex fluor-488, donkey anti-goat or goat anti-mouse IgG conjugated with Alex fluor-594 (1:1000, abcam, ab150061, ab150081, ab150136, ab150120, Waltham, MA, USA) for 2 h at room temperature. After washing thrice with PBST, the sections were mounted on a slide and covered with a mounting medium containing DAPI (Abcam, ab104139, Waltham, MA, USA). Dual labeling immunofluorescence staining of c-Fos and CGRP was performed to clearly locate c-Fos-positive cells in the superficial layer of the SPVC delineated by the CGRP fluorescent signal. Five SPVC sections (from 7.8 mm to 8.2 mm posterior to the bregma) from each animal were selected to image using a confocal microscope (Olympus FV1000). All images were acquired at 1,024 × 1,024 resolution using 2× Kalman frame averaging. High-resolution z-stacks were acquired using a 40×oil-immersion lens at a step size of 3 μm. The number of c-Fos positive cells was counted manually and the integrated density of CGRP was measured with ImageJ software (Fiji, NIH, USA). For cellular localization of ANXA1 in the SPVC, the sections were first treated with 51% Triton X-100 for 60 min to rupture the cell membranes before incubating with blocking buffer.

### RNA-seq

Mice from the four groups were sacrificed on day 40 without BLS. The bilateral SPVC was dissected under RNase-free conditions for RNA-Seq. Total RNA was isolated from the SPVC using the TRIzol method (15596018, Invitrogen, CA, USA) according to the manufacturer's protocol. We used 1.5 μg RNA per sample as input material for RNA sample preparations. Sequencing libraries were generated using NEBNext Ultra RNA Library prep Kit for Illumina (E7770, New England Biolabs, USA) following the manufacturer's recommendations. Index codes were added to attribute sequences to each sample. Briefly, the mRNA was enriched and cleaved into short fragments using divalent cations under elevated temperature in NEBNext First Strand Synthesis Reaction Buffer (5X), followed by reverse transcription into cDNA using a random hexamer primer. The cDNA fragments were purified, end-repaired, their 3′ ends were adenylated, and ligated with NEBNext Adaptor with hairpin loop structure. The ligation products were then size selected using USER Enzyme (M5505, New England Biolabs, USA). Then, PCR was performed with Phusion High-Fidelity DNA polymerase (M0530L, New England Biolabs, USA), universal PCR primers and index (X) primer. Finally, the library preparations were sequenced on an Illumina Novaseq 6000 platform by the Beijing Allwegene Technology Company Limited (Beijing, China) and paired-end 150 bp reads were generated.

Raw data (raw reads, SRA: PRJNA979279) in fastq format were first processed using in-house perl scripts. Clean data (clean reads) were obtained by removing reads containing adapter, reads containing ploy-N, and low-quality reads from raw data. The Q20, Q30, GC-content and sequence duplication level of the clean data were calculated. All the downstream analyses were conducted using clean, high-quality data.

### Differentially expressed gene analysis

HTSeq (v 0.13.5)[58] was used to count the read numbers mapped to each gene. The gene expression levels were estimated by fragments per kilobase of transcript per million fragments mapped (FPKM). Differential expression analysis of each two compared groups was performed using the DESeq R package (1.12.1).[59] The resulting p values were adjusted using the Benjamini and Hochberg's approach for controlling the false discovery rate. Genes with an adjusted p value <0.05 found by DESeq with an absolute fold change of 2 or more were considered differentially expressed. Volcano plot, venn diagram, and clustering correlation heatmap with signs were created with the OmicStudio tools (https://www.omicstudio.cn/tool). Distances of expressed genes were calculated using the Euclidean method.

### Quantitative RT-PCR

Bilateral SPVC tissues from the four groups were harvested on day 40 without BLS and shock-frozen on dry ice. The total RNA was extracted from the SPVC tissue using TSINGKE TSP413 RNAprep FastPure (Tsingke Biotechnology Co., Ltd., TSP413, Beijing, China) in accordance with the manufacturer's protocol. RNA extracts were reverse transcribed using Goldenstar RT6 cDNA Synthesis Kit Ver 2 (Tsingke Biotechnology Co., Ltd., TSK302S, Beijing, China). The cDNAs were then amplified via quantitative RT-PCR using 2×T5 Fast qPCR Mix (SYBR Green I) (Tsingke Biotechnology Co., Ltd., TSE202, Beijing, China) with 20 μL reaction system on a Real-Time PCR System (Bioer Technology, FQD-96A, Hangzhou, China), normalized to GAPDH. Relative quantification was determined using the ΔΔCT method. primer sequences are listed in Table 2.

### Western blot

Bilateral SPVC tissues from the four groups were harvested on day 40 without BLS and shock-frozen on dry ice. For total protein extraction, SPVC tissues were homogenized in RIPA lysis buffer (Beyotime Biotechnology, p0013B, Shanghai, China) containing phenylmethylsulphonyl fluoride (Beyotime Biotechnology, ST506, Shanghai, China) and protease inhibitor (Roche, 05892970001, Basel, Switzerland) with homogenizer workcenter (IKA-Werke GmbH & CO. KG, 0003737025, Beijing, China) on ice, and centrifuged at 12,000 rpm for 15 min at 4°C. The total protein concentration was measured using the BCA protein Assay Kit (Beyotime Biotechnology, p0010S, Shanghai, China). An aliquot of the supernatant was taken and normalized to 2.5 μg/μL in 5× SDS-PAGE loading buffer (Beyotime Biotechnology, p0015L, Shanghai, China) and double distilled water and heated at 95°C for 8 min. SDS-PAGE was performed using 10%–15% bis/tris polyacrylamide gels; 25 μg protein was loaded in each lane. The proteins were then electrophoretically transferred to polyvinyl difluoride membranes (Millipore Merck Chemicals (Shanghai) Co., Ltd, IPVH00010, Shanghai, China). The membranes were blocked with 5% non-fat milk at room temperature for 1 h, followed by overnight incubation at 4°C with the following primary antibodies: rabbit anti-ANXAI (1:1000, Abcam, ab214486, Waltham, MA, USA) and mouse anti-α-tubulin (Beyotime Biotechnology, AF2827, Shanghai, China). The next day, the membranes were incubated with a horseradish peroxidase-conjugated anti-mouse secondary antibody (1:5000, Beyotime Biotechnology, A0216, Shanghai, China) and horseradish peroxidase-conjugated anti-mouse/rabbit secondary antibody (1:5000, Beyotime Biotechnology, A0216, A0208, Shanghai, China) at room temperature for 1 h. proteins were visualized with a Super ECL plus Kit (Wansheng Haotian Biotechnology Co., Ltd, EZWB01, Shanghai, China) on a Tanon 5200 chemiluminescent imaging system (Tanon, China). The scanned images were quantified using ImageJ software. The expression level of ANXA1 was normalized to its α-tubulin loading control.

### Cannula implantation and drug intracerebroventricular microinjection

On day 30, after being anesthetized with 1.25% avertin, GTN+RIZ/VEH+SAL mice were placed on a stereotaxic device (RWD Life Science, 69105, Shenzhen, China). A stainless steel guide cannula (26 gauge, RWD Life Science, 62003, Shenzhen, China) was implanted into the right lateral ventricle at the coordinates anteroposterior [AP] −0.46 mm, mediolateral [ML] −1 mm, and dorsoventral [DV] −1.8 mm according to the paxinos & Franklin Mouse Brain Atlas.[62] The cannula was anchored to the skull with dental cement. Then, the mice were allowed to recover from surgery for 10 days.

Intracerebroventricular (i.c.v.) microinjection was performed with a 25 μL Hamilton microliter syringe, which was connected to an injection cannula (RWD Life Science, 62203, Shenzhen, China) via a polyethylene tube and driven by a syringe pump (KD Scientific, 788130, USA). Drugs were injected at a volume of 5 μL/mouse, and at a speed of 0.5 μL/min. After the expected volume was injected, 5-min delay time was allowed for the drug to diffuse. During drug infusion, the mice were maintained under light isoflurane (1%–1.5%) anesthesia. The ANXA1-derived active peptide Ac2-26 TFA (Ac-AMVSEFLKQAWFIENEEQEYVQTVK, MedChemExpress LLC, HY-P1098A, Shanghai, China) was freshly diluted with 0.9% saline for a dose of 5 μg/mouse and administered immediately after sonication. An equal volume of saline was used as control. The stock solutions of the formyl peptide receptor (FPR) antagonist Boc-MLF TFA (MedChemExpress LLC, HY-103473A, Shanghai, China) were prepared by dissolving it in dimethyl sulfoxide. Aliquots of this solution were subsequently diluted in saline (dimethyl sulfoxide:saline 1:99, v/v) for i.c.v. treatment at a dose of 1 μg/mouse. The dose of these two drugs was determined based on previous study.[24] On day 40, Ac2-26 TFA was administered 30 min before the mice were exposed to BLS, and Boc-MLF TFA was infused 20 min before the administration of Ac2-26 TFA. The location of the cannula was verified histologically by sectioning the brain after infusing Evans Blue (E2129, Sigma). The representative location of the cannula is shown in Figure S2.

## QUANTIFICATION AND STATISTICAL ANALYSIS

All behavioral testing and data analyses were performed by experimenters who were blinded to mice treatments. Sample sizes were determined according to the investigator's experience and previous studies.[10,63] All data were presented as mean ± standard error of the mean. Two-way repeated-measures analysis of variance (ANOVA) with Tukey post hoc test, one-way repeated-measures ANOVA with Dunnett post hoc test, one-way ANOVA with Tukey post hoc test and paired *t* test were performed using Graphpad prism 8 (Graphpad Software, La Jolla, CA, USA). The details of the statistical analyses used for different experiments are described in the figure legends. A p value of $<0.05$ was considered statistically significant.